AD-761 599

THE PENETRATION OF A FLUID SURFACE BY
A WEDGE

John D. Pierson

Institute of the Aerospace Sciences, Incorporated
New York, New York

July 1950

The Penetration of a Fluid Surface by a Wedge

By

JOHN D. PIERSON
Consultant

Experimental Towing Tank
Stevens Institute of Technology

A Sherman M. Fairchild Publication Fund Paper

By the

INSTITUTE OF THE AERONAUTICAL SCIENCES

64

THE PENETRATION OF A FLUID SURFACE

BY A WEDGE

REPORT NO. 381

by

John D. Pierson, Consultant

July 1950

TABLE OF CONTENTS

PAGE

SUMMARY

Several basic conditions which determine the shape of the free fluid surface due to the vertical immersion of an infinite wedge in a perfect fluid are analyzed. Continuity of the fluid flow, dynamic similarity, and finally the conditions for irrotational potential flow are applied to estimated surface shapes until, by an iterative solution method, a unique surface shape is obtained for a given wedge angle. This method of analysis is carried out for several wedges (deadrise angles up to 50°), and the corresponding free surface shapes are constructed in detail. Empirical formulae for the relative spray thickness are also given.

Knowledge of the free surface shape enables a solution for the velocity and potential everywhere on the free surface, and also in the wedge itself. From these data, the impact force and pressure distribution on the wedge are computed. Comparison of the pressures with a previous simpler analysis based on an analogy with the flow around an expanding flat plate shows reasonable agreement at low angles, but a large percentage reduction in pressure at high deadrise angles.

The study was made at the Experimental Towing Tank, Stevens Institute of Technology, under the sponsorship of the Office of Naval Research, Department of the Navy.

INTRODUCTION

This report is one of a series prepared at the Experimental Towing Tank, Stevens Institute of Technology, in connection with the research on planing surfaces conducted under Contract No. N6onr-247, Task Order IV, with the Office of Naval Research. The research project, which includes theoretical and experimental investigations on the problem of planing on the surface of water, is divided into two general groupings:

a) Investigation of the fundamental nature of the hydrodynamic planing process.

b) Collection and organization of seaplane and flying-boat design data for the establishment of rational design methods and for comparison with theoretical results.

Group (a) is primarily of a theoretical or mathematical nature, dealing with the detailed fluid flow in the vicinity of a planing surface. Results of these theoretical studies are presented in References 1, 2, and 3, with additional reports in the process of preparation. Group (b) is primarily experimental and empirical, dealing with an over-all evaluation of the effects of the many parameters that influence the planing process. Results of the empirical studies completed to date are presented in References 4, 5, 6, and 7.

The present report is a portion of the investigation into the fundamental nature of the hydrodynamic planing process. It deals in detail with the rise of the surface, formation of spray, pressures, and loads which occur during the normal penetration of a fluid surface by an infinite wedge.

The general appearance of the spray and wave surface which results from the penetration of a fluid surface by a wedge shape has been experimentally noted by many observers. However, the transitory nature of the problem and the small measurements involved have made accurate experimental data difficult to obtain. Loads and pressure distributions for wedge immersions have been determined experimentally (because of the importance of the problem in seaplane design), but only at the expense of intricate and costly test procedures.

Analysis and understanding of the experimental data obtained have been hampered by a lack of a basic analytical solution to the penetration problem. The earlier work of Wagner (Reference 8), brief and cryptic as it is, has nevertheless provided a groundwork for the theoretical study of the many problems associated with planing and impact. Previous reports of this series have amplified and extended Wagner's analyses for the detailed flow in the spray-root and trailing-edge regions and, by the expanding-plate analogy, for the loads and pressures on a wedge penetrating the fluid surface. These analyses were limited to relatively low angles by the assumptions required for their solutions. The removal of the restriction to low deadrise angle would make the results of these theoretical studies of greater practical engineering value.

It is the purpose of this report to present the more general method of analysis suggested by Wagner which yields the free surface shape and associated pressures and loads during the symmetrical penetration of a fluid surface by a wedge of any angle.

SYMBOLS

a,b points on free surface of fluid; also distance of points from origin o

c nominal wetted half-width

d subscript pertaining to doublet

id subscript pertaining to image doublet

k U/V at point on surface

n distance normal to free surface, + inward

o origin of x,y axes

o' edge of spray, origin for s

p pressure at any point in flow field $[-\rho(\partial\phi/\partial t) - \rho(U^2/2) + \rho F(t)]$

R distance to doublet center

r distance from origin to point in fluid (usually on surface curve)

s distance along surface from its origin at solid boundary (Figure 2); also general point on free surface or wedge

t	time
U	resultant velocity at any point $\sqrt{u^2 + v^2}$
u	velocity component $\parallel x$ axis; $\leftarrow \rightarrow$; $\partial\phi/\partial x$, $\partial\psi/\partial y$
V	velocity of wedge or field velocity at ∞
v	velocity component $\parallel y$ axis; $+ \uparrow$; $\partial\phi/\partial y$, $-\partial\psi/\partial x$
x	horizontal distance to $\oint$ symmetry
$\bar{x}$	position of peak pressure on bottom
y_0	vertical distance to apex of wedge (from undisturbed water surface)
α	angle between velocity vector, U, and radius, r
β	angle of deadrise (as a subscript, denotes polar coordinate *system* (Figure 7))
γ	angular orientation with respect to doublet
δ	spray thickness
ζ	angle between the radial velocity and the surface velocity past the radius
η	y coordinate of particular fluid particle(especially surface particles)
θ	angle between radius from doublet and free surface at any point
μ	angle subtended at the doublet by the line $y_0 o'$
ξ	x coordinate of particular fluid particle (especially surface particles)
ρ	mass density of fluid
ϕ	velocity potential
ψ	stream function
∇	differential operator ($\nabla\phi = \text{grad}\phi$)
∇^2	Laplacian operator $=$ div grad

THEORETICAL ANALYSIS

CONDITIONS OF THE PROBLEM

The problem is treated as a two-dimensional one, and the infinite wedge is assumed to be symmetrical about the vertical centerline plane, and perfectly rigid. For this first analysis, the velocity of penetration is taken as a constant (very high mass or forced penetration).

The fluid is assumed incompressible and frictionless. The flow field is assumed to be initially irrotational, and thus must remain so under the first assumption of the perfect fluid. The velocity of penetration is assumed to be sufficiently high and the size of the wedge great enough that the effects of gravity and surface tension may be safely neglected.

The initial penetration of the wedge splits the previously undisturbed fluid surface into two surface sheets. On the basis of the assumptions of perfect fluid and irrotational flow, it follows that particles on the original surface remain and no new particles are added (Reference 9) and, since the fluid is incompressible, the surface as deflected by the wedge penetration must have a constant length of arc.

These conditions correspond to the requirements for a potential

flow. For convenience in application to the problem, however, three conditions are abstracted which define the shape of the free surface:

1) Continuity: The fluid displaced by the wedge must appear above the original water surface in the form of a wave and/or spray (incompressibility), and the arc length of the surface must be constant.

2) Similarity: Since the wedge is symmetrical and the immersion is normal to the undisturbed surface, the field of flow is divided into two halves by the centerline of symmetry. The neglect of gravity forces and scale effects leads to the definition of surface shape and dynamic state of the field of flow entirely in terms of the wedge penetration (distance and velocity). At constant penetration velocity, the flow field and surface shape must then be geometrically and dynamically similar at all times.

3) Irrotationality: The fluid flow field may be represented by the potential function, ϕ. For irrotational flow, the relation $\nabla^2 \phi = 0$ must be satisfied everywhere in the flow field, where ∇^2 is the Laplacian operator div grad.

METHOD OF APPLICATION OF GENERAL CONDITIONS

CONTINUITY

There are any number of possible solutions for the free surface shape on the basis of continuity alone. Two extreme solutions are shown in Figure 1: one limiting case is all wave with infinitesimally thick spray, while the other is the opposite -- all spray and no wave. Between these extremes lie the combinations of various spray and wave shapes as indicated in Figure 2.

One analytic expression for the 'all wave' condition is obtained from the equations of flow about a flat plate as given in References 3 and 8. From consideration of the potential flow about a flat plate, with the flat-plate width treated as a variable, it is possible to determine the velocity distribution and then the effective surface rise in the plane of the plate (as shown in Figure 1). This solution gives an analytic expression for the wave rise, η. The rate of expansion of the plate determines the equivalent deadrise, β, to which this analytic solution is assumed to apply. It is simple to demonstrate by integration of the area under the wave that the continuity condition is satisfied.

From Figure 1, the areas A and B for the 'all wave' condition are

$$A = \frac{\tan\beta}{2}\left(\frac{2}{\pi}c\right)^2 \tag{1}$$

and

$$B = \frac{\tan\beta}{2}\left(c - \frac{2}{\pi}c\right)^2 + \int_c^\infty \eta\,dx \quad . \tag{2}$$

From Equation 38 of Reference 8, (or Equations 11 and 13 of Reference 3), the wave rise η is given by:

$$\eta = \frac{2\tan\beta}{\pi} x \, \arcsin\frac{c}{x} - \frac{2\tan\beta}{\pi} c \tag{3}$$

$$\int_c^\infty \eta\,dx = \frac{\tan\beta}{2} c^2 \int_c^\infty \left(\frac{4x}{\pi c^2} \, \arcsin\frac{c}{x} - \frac{4}{\pi c}\right) dx$$

$$= \frac{\tan\beta}{2} c^2 \left[\frac{2x^2}{c^2} \arcsin\frac{c}{x} + \frac{2}{\pi c}\sqrt{x^2 - c^2} - \frac{4x}{\pi c}\right]_c^{x-\infty}$$

$$= \frac{\tan\beta}{2} c^2 \left[-\left(1 - \frac{4}{\pi}\right)\right] \quad . \tag{4}$$

Therefore, combining Equations (2) and (4) gives:

$$B = \frac{\tan\beta}{2} c^2 \left(1 - \frac{2}{\pi}\right)^2 + \frac{\tan\beta}{2} c^2 \left(\frac{4}{\pi} - 1\right)$$

$$= \frac{\tan\beta}{2} c^2 \left(\frac{2}{\pi}\right)^2 \quad , \tag{5}$$

which is equivalent to the expression for the area A.

The 'all spray' condition could be solved directly by simultaneous equations for the area and length equalities required by the continuity condition:

$$A = B \qquad \text{and} \qquad oa = o'a \quad . \tag{6}$$

However, these two cases are evidently not real possibilities because of the sharp fluid corner which would be required either at the wedge or at the still water surface. They merely represent the extremes between which an infinite variation of wave and surface shape may occur.

In general, any thickness of spray may be associated with an un-limited variety of waves and still not violate the continuity requirement.

SIMILARITY

The principle of similarity for the proportional increase of the wave and spray with continued penetration is the second basic considera-tion. Not only must the displaced fluid appear above the initially undis-

turbed surface, but the wave and spray must be increasing in such a manner that the shape and velocities are everywhere determined by the position and penetration velocity of the wedge. By a geometrical construction and integration process proposed by Wagner (Reference 8), it is possible to relate the surface shape and velocities so that for any spray thickness, one corresponding wave and spray-root shape which meets the requirements of similarity and continuity is determined.

In an ideal fluid where gravity, viscosity, and surface tension effects are neglected, the shape of the free surface is uniquely determined by the shape of the body, and the size of the shapes is determined by the amount of penetration. Thus, for a simple wedge penetration, the free surface shape is always the same.

For the same relative positions in the fluid and on the surface, the dynamic conditions of pressure and velocity depend upon the surface shape and must bear the same relationship to the penetration velocity at every instant of time. It should be noted that this statement applies to a relative position in the fluid and not to a particular fluid element since, as it will be shown later, particular particles move from one position to another and are subject to varying pressure and velocity with the passage of time

For example, consider the several stages of the penetration process illustrated in Figure 3. Initial contact is made at point o, splitting the surface layer. Penetration into the fluid raises the initially flat surface into a wave and deflects the nearby particles out along the wedge surface as spray. (The transition area where the wave surface is rapidly curved around into the spray is termed the spray root.) The resulting surface shape expands with the penetration of the wedge as indicated by the several positions $o'_1 a_1 b_1 c_1$, $o'_2 a_2 b_2 c_2$, and $o'_3 a_3 b_3 c_3$.

Under the assumed perfect properties of the fluid, such a series of scalar curves for a constant velocity immersion could just as well be represented by any one of the curves, the scale of the *diagram* then depending on the wedge penetration. Since the fluid particles are not restricted in size, the scale of the diagram is of no consequence. Thus, the radiating lines oa, ob, etc. define corresponding points on the surfaces for similitude since the point o is the origin of the motion.

(It is interesting to note that several points other than the origin chosen could be used as a center of symmetry for the expanding surface. The wedge apex, y_o, the spray tip, o', or the intersection of the wedge side with the still water surface could be considered as points of origin for the expansion of the flow. However, the latter two would appear as double centers for the complete wedge, and all three have the disadvantage that the 'center' of the expansion would be moving with respect to the initial penetration point and with respect to the fluid at a great distance from the wedge. Since such motions of the center of expansion would complicate the problem unnecessarily, the initial contact point, o, will be used.)

Corresponding points on the surface are determined by the ratios:

$$\frac{o'_1 a_1}{oa_1} = \frac{o'_2 a_2}{oa_2} \quad ; \quad \frac{o'_2 b_2}{ob_2} = \frac{o'_3 b_3}{ob_3} ; \text{ etc.} \tag{13}$$

Also, the velocity at corresponding points must be equal:

$$U_{a_1} = U_{a_2} = U_{a_3} = k_a V ; \quad U_{b_1} = U_{b_2} = U_{b_3} = k_b V; \text{ etc.,} \tag{14}$$

where k_a, k_b, etc represent the proportionality factors between the velocity U at positions a, b, etc., and the penetration velocity, V.

At any point on the surface, say c_3, the velocity is determined from consideration of this condition of similarity. From the instant of contact, the surface may be considered to have been sliding past the radius oc in a direction tangent to the surface at c_3, at a rate sufficient to maintain the ratios in Equation (13). Thus, a particle at the surface (at point c_3) is momentarily moving with the expansion of the radius, and at the same time sliding past the radius towards the spray region. The vector sum of these two motions $(U_{r_c} + U_{s_c})$ yields the resultant velocity U_c of the particle at the point in question.

The radial expansion velocity, U_r, and the surface velocity past the radius, U_s, as well as the resultant velocity, U, are each directly proportional to the penetration velocity, V (Equation (14)). Thus, for constant penetration velocity, V, the velocity components (U_{r_c} and U_{s_c}) at position c are constant, and the vector sum of the velocities may be obtained from the radial distance and the arc length:

The radial distance $oc_3 = r$ is given by:

$$r = \int_o^t U_{r_c} \, dt = U_{r_c} t.$$

The vector s is constructed tangent to the surface at c so that s equals the arc length $o'c$:

$$s = \int_o^t U_{s_c} \, dt = U_{s_c} t.$$

The vector sum is then:

$$s + r = \int_o^t U_c \, dt = U_c t . \tag{15}$$

Now the actual fluid particles on the surface do not follow the radiating lines but remain at a fixed arc length from the split edge of the surface, o'. For example, a particle initially at rest at (ξ_o, o) rises first as a part of the wave surface and later becomes a part of the spray. The velocity of the particle varies with its position on the sur-

face. The motion of the particle is thus a function of its relative position and is given at any time by the integral relation:

$$(\xi - \xi_o, \eta) = \int_0^t U_{(\xi,\eta)} \, dt \; , \tag{16}$$

or more specifically,

$$\xi - \xi_o = \int_0^t u_{(\xi,\eta)} \, dt \tag{16a}$$

$$\eta = \int_0^t v_{(\xi,\eta)} \, dt \quad . \tag{16b}$$

The problem is to determine the velocity of the particle $(\dot\xi, \eta)$ at any point in its path, and then to relate the position and time so that the integral may be solved. This does not appear to have an analytic solution, but the graphical solution is easily carried out.

The velocity of the particle (ξ, η) may be found directly at any particular time by constructing the surface of the proper penetration, locating the point according to its arc length from o', and performing the vector addition of Equation (15). However, this would be a tedious process to determine enough points for step-by-step integration of Equation (16). A more simple alternate method is to change the variable from time to arc length, which is done in the following manner.

Assume particle (ξ, η) at time t_2 to be at position c_2. Then, at t_2, $U_\xi = U_{c,\eta}$ which may be determined on the t_3 curve at c_3. In other words the surface points $d_3 c_3 b_3$ correspond to earlier times on the particle path. The time t_2 is related to t_3 by the arc lengths at corresponding points c_2 and c_3.

$$\frac{s_{c_3}}{t_3} = U_{s_c} = \frac{s_{c_2}}{t_2} = \frac{s_o}{t_2}$$

or, in general, with t = the earlier time t_2, and s = the corresponding arc length on the surface at time t_3:

$$t = \frac{s_o t_3}{s}$$

and

$$dt = -\frac{s_o t_3}{s^2} \, ds \quad .$$

Substitution for dt in Equations (16a) and (16b) gives

$$\xi - \xi_0 = \int_{x}^{s_0} u_{\xi,\eta} \left(-\frac{s_0 t_3}{s^2} ds \right) = s_0 \int_{s_0}^{\infty} \frac{u t_3}{s^2} ds \tag{17a}$$

and

$$\eta = s_0 \int_{s_0}^{\infty} \frac{v t_3}{s^2} ds . \tag{17b}$$

The horizontal and vertical components, ut and vt, may be found at any point along the surface by using Equation (15), and a step-by-step integration of the above formulae may be accomplished. Any trial curve which satisfies the continuity condition may be used as a starting point for the determination of the surface velocities. The solution of Equations (17a) and (17b) determines a new curve which is used in turn to obtain revised values of the velocity components. This iterative process is continued until negligible differences occur between computed and trial curves of surface shape.

Actually, the integral equations relate the rise at a particular point to all the points more distant from the wedge. Thus, the path of each point on the surface follows the same related pattern, and the surface shape fits the requirements for similarity. Although rigorous analytical proof is omitted, it appears from the actual computations which have been made that the integral relationship (Equations (17a) and (17b)) reduces the number of possible spray-wave combinations to one for each spray thickness.

POTENTIAL AND STREAM FUNCTION ON THE FREE SURFACE

For use in the application of the third condition, which follows, a potential function that satisfies the first two conditions is assumed to exist for the fluid field of each spray-wave combination (even though such an assumption can be true only for the one free surface shape which meets all the conditions of the problem). The values of the potential ϕ and the stream function ψ on the free surface may be found as follows.

In Figure 3, the tangential velocity, $\partial\phi/\partial s$, along the surface at a position c is given by $-U_{s_c} + U_{r_c} \cos\zeta$. In terms of the potential ϕ, the tangential velocity $= \partial\phi/\partial s$. For points along the surface (at fixed immersion), $\cos\zeta$ is given by dr/ds. (The values of dr/ds for the particular surface, such as 3, should not be confused with $dr/ds = r/s$ for a constant position, such as c.) Then

$$-\frac{\partial\phi}{\partial s} = U_{s_c} - U_{r_c} \cos\zeta = U_{s_c} - U_{r_c} \frac{dr}{ds} \tag{18}$$

The general differential equation is obtained by multiplying Equation (18) by $t\, ds$ and dropping the subscript c (noting that $t U_s = s$ and $t U_r = r$)

$$-t \, d\phi = s \, ds - r \, dr \qquad (19)$$

Integration gives

$$-t\phi = \frac{(s^2 - r^2)}{2} + A \quad . \qquad (20)$$

Since $\phi = 0$ at $s = r = \infty$, $A = 0$ and

$$\frac{\phi}{t} = \frac{r^2 - s^2}{2t^2} = \frac{U_r^2 - U_s^2}{2} \qquad . \qquad (21)$$

The stream function ψ on the free surface is found in a similar manner. At position c, the normal velocity is given by $U_{r_c} \sin\zeta$. In terms of ψ,

$$-\frac{\partial\psi}{\partial s} = U_{r_c} \sin\zeta \quad .$$

Multiplication by $t \, ds$ gives:

$$t \frac{\partial\psi}{\partial s} ds = r_c \sin\zeta \, ds \quad .$$

The integration of the right-hand side is accomplished graphically since it represents the area swept out by the radius r. Thus,

$$\int_{\psi=\psi_{o'}}^{\psi=\psi_c} t \frac{\partial\psi}{\partial s} ds = -2 \, (\text{area } oo'co)$$

and in general terms, the general position s replaces the particular point c, and

$$t \, \psi_s = t \, \psi_{o'} - 2 \, (\text{area } oo'so) \quad .$$

For $\psi = 0$ on the centerline of symmetry, $t\psi_o$ is determined by the constant normal component of the velocity at the wedge surface, U_n:

$$U_n = V \cos\beta \quad ,$$

$$t \, \psi_{o'} = t \, (\overline{y_o o'}) \, V \cos\beta = (\overline{y_o o'}) \, y_o \cos\beta = 2 \, (\text{area } oo'y_o o)$$

and thus

$$t \, \psi_s = 2 \, (\text{area } oo'y_o o - \text{area } oo'so) \quad . \qquad (22)$$

It will be noted that as $s \to \infty$, the area $oo'so$ becomes equal to the area $oo'y_o o$ by virtue of their common area and the condition of continu-

ity. Thus, $\psi_x = 0 = \psi_{y_o}$, which is as it should be.

IRROTATIONALITY

Irrotational potential flow is the final condition for the field of the wedge penetrating the fluid surface. Everywhere within the fluid and on the boundaries, the requirement must be satisfied that $\nabla^2\phi = 0$. This may be written in several equivalent forms:

$$\nabla^2\phi = \frac{\partial^2\phi}{\partial x^2} + \frac{\partial^2\phi}{\partial y^2} = \frac{\partial^2\phi}{\partial n^2} + \frac{\partial^2\phi}{\partial s^2} = \frac{\partial U_n}{\partial n} + \frac{\partial U_s}{\partial s} = 0 . \tag{23}$$

From the graphical constructions made for the condition of similarity, it is possible to obtain ϕ, U_n, U_s, and even $\partial U_s/\partial s$ along the free surface boundary; but $\partial U_n/\partial n$ is not obtainable, and no interior values may be found. Therefore, it is not possible to use Equation (23) as a direct check on the surface shapes obtained through application of the first two conditions. Instead, an indirect method of approach is used, based on Greene's theorem (Reference 9).

Greene's theorem, which relates surface integrals to volume integrals for superimposed potential flows, states that for irrotational potential flows:

$$\oint_S \phi_1 \frac{\partial\phi_2}{\partial n} ds = \oint_S \phi_2 \frac{\partial\phi_1}{\partial n} ds , \tag{24}$$

where ϕ_1 and ϕ_2 are any two irrotational, potential flows superimposed in a common region S, and the integral is taken over the boundary surface of the region only. If the known irrotational potential function for a doublet, ϕ_d, is chosen for ϕ_1, and $\phi_2 = \phi$ (the questionable value determined from the free surface shape), the integrals will check only if ϕ is also a potential function for an irrotational flow.

The doublet may be located anywhere on the assumed free surface. However, the field of a doublet decreases rapidly with distance, and the choice of location for this checking purpose may be quite critical. Since the largest deviation from irrotational potential flow could be expected in the spray-root region, the doublet is located in this region as shown in Figure 4. (It is necessary to add the image doublet above the wedge to give $\partial\phi_d/\partial n = 0$ on the wedge surface, because the graphical construction which satisfies the similarity condition does not yield any information on the potential along the wedge.)

Consider the flow in the immediate area of the doublet as shown in Figure 5, an enlarged section of Figure 4. The field of the doublet is given by

$$\phi_d = \frac{\sin\alpha}{R} , \tag{25}$$

from which the velocities due to this field are given by

$$\frac{\partial \phi_d}{\partial R} = -\frac{\sin\alpha}{R^2} \tag{26}$$

$$\frac{\partial \phi_d}{R\,\partial\alpha} = \frac{\cos\alpha}{R^2} \quad . \tag{27}$$

At the free surface, the normal component is given by

$$\frac{\partial \phi_d}{\partial n} = \sin\theta \frac{\partial \phi_d}{\partial R} - \cos\theta \frac{\partial \phi_d}{R\,\partial\alpha} = \frac{1}{R^2}(-\sin\theta \sin\alpha - \cos\theta \cos\alpha)$$

$$= -\frac{\cos(\alpha - \theta)}{R^2} \quad . \tag{28}$$

The potential and velocity equations for the image doublet are the same as the above except that α and θ are interpreted as positive in the counter-clockwise direction (and of course the R values are measured to a different center).

On the ₵ below the wedge apex, the doublets do not exactly balance because of the change in angle between the wedge bottom and the ₵. Since, at this distance, the velocities due to the doublet or its image are small (as $1/R^2$), the net difference normal to the ₵ is very small and may be safely neglected.

The surface integral required to check the $\nabla^2\phi$ condition may be evaluated from the known potential field of the doublets and the measured field characteristics of the assumed surface shape by breaking the surface into a number of segments:

$$\oint_c = \int_{₵^\infty}^{\substack{x=0\\y=y_0}} + \int_{\substack{z=0\\y=y_0}}^{s=0} + \int_{s=0}^{s=s_d-\epsilon} + \int_{s_d=}^{s_d+\epsilon} + \int_{s=s_d+\epsilon}^{s=\infty} + \int_{s=\infty}^{₵^\infty} \quad .$$

The evaluation of the integral on each segment will be discussed separately and reduced to its simplest form before writing Equation (24) in its entirety.

The portion of the surface integral on the ₵ of symmetry below the wedge apex is represented by

$$\int_{₵^\alpha}^{x=0,\ y=y_0} \quad .$$

This portion of the integral may be shown to be convergent to a small value, which may be safely neglected. Over the part of the surface $\partial\phi/\partial n = 0$, ϕ_d is small (on the order of $1/R$), and

$$\int_{\infty}^{0} (0)\ (\sin\alpha/R)\ ds = 0$$

for $s \rightarrow R$ at infinity. Also, $\partial\phi_d/\partial n$ for one doublet is very small at and below y_o (on the order of $1/R^2$). For the pair of doublets, the value is the difference between the two, an even smaller value. On the $\cline$ below the wedge, ϕ is not given by the analysis so far, but from the expanding-plate analogy (Reference 3), the value is on the order of R_{y_o} at the wedge apex, and diminishes rapidly below the wedge, giving

$$\int_{\alpha}^{y=y_o} R_{y_o}\ \frac{\cos\ (\alpha - \theta)}{R^2}\ ds\ ,$$

which is convergent for $s \rightarrow R \rightarrow \infty$. Since the small finite value which might accrue from this integral appears to be much lower than the mechanical accuracy of the graphical method to be used, this term may be neglected.

The value of the integral along the solid boundary from wedge apex to spray tip,

$$\int_{\substack{x=0 \\ y=y_o}}^{s=0}\ ,$$

may be determined analytically. Along the wedge, ϕ is not known, but is finite, while $\partial\phi_d/\partial n = 0$, so that

$$\int_{y_o}^{o'} \phi\frac{\partial\phi_d}{\partial n}\ ds = 0.$$

The doublet and its image add along the wedge:

$$\phi_d = 2\frac{\sin\alpha}{R}\ .$$

Since $\partial\phi/\partial n = V\cos\beta$ and $ds = R\ d\alpha/\sin\alpha$,

$$\int_{y_o}^{o'} \phi_d\frac{\partial\phi}{\partial n}\ ds = \int_{\alpha y_o}^{\alpha o'} 2\ V\ \cos\beta\ d\alpha = 2\ V\ \mu\cos\beta\ ,$$

where μ is $\oint y_o d o'$.

Two terms

$$\int_{s=0}^{s=s_d-\epsilon} \quad \text{and} \quad \int_{s=s_d+\epsilon}^{s=x}$$

which represent the integrals on the free surface from the spray tip to

the doublet and from the doublet to infinity are indicated because the free surface is theoretically broken for a distance 2ϵ at the doublet $(s = s_d)$. At all other points of the free surface, ϕ and $\partial\phi/\partial n$ are given by constructions for the assumed surface, and ϕ_d and $\partial\phi_d/\partial n$ are given by Equations (25) and (28). Because of the discontinuity at the doublet center, a small semi-circular path is followed around the singular point to obtain

$$\int_{s_d-\epsilon}^{s_d+\epsilon} .$$

(The distance 2ϵ is taken so small that the effect of the image doublet is infinitesimal.) The doublet potential and normal velocity components are given by Equations (26) and (27). The potential and normal velocity of the main flow field are obtained on this small semi-circular segment by assuming no variation of the field velocity for the small area involved. As shown in Figure 5,

$$\phi = \phi\Big|_d + R\cos\frac{\partial\phi}{\partial R} \quad (\text{for } R \to \epsilon \text{ only})$$

and

$$\frac{\partial\phi}{\partial R} - \cos\alpha\frac{\partial\phi}{\partial n}\Big|_d - \sin\alpha\frac{\partial\phi}{\partial s}\Big|_d .$$

where $\big|_d$ indicates a constant value for the main flow field in the immediate region of the doublet. Thus,

$$\phi = \phi\Big|_d + R\cos\alpha\frac{\partial\phi}{\partial n}\Big|_d - R\sin\alpha\frac{\partial\phi}{\partial s}\Big|_d$$

and

$$\int_{s_d-\epsilon}^{s_d+\epsilon} \phi_d\frac{\partial\phi}{\partial n}\,ds - \int_{\pi/2}^{-\pi/2} \phi_d\frac{\partial\phi}{\partial R}R\,d\alpha$$

$$-\int_{\pi/2}^{-\pi/2} \left(\frac{\sin\alpha}{R}\right)\left(\cos\alpha\frac{\partial\phi}{\partial n}\Big|_d - \sin\alpha\frac{\partial\phi}{\partial s}\Big|_d\right)R\,d\alpha$$

$$\cdot - \frac{\pi}{2}\frac{\partial\phi}{\partial s}\Big|_d .$$

Also:

$$\int_{s_d-\epsilon}^{s_d+\epsilon} \phi \frac{\partial \phi_d}{\partial n} ds = \int_{\pi/2}^{-\pi/2} \phi \frac{\partial \phi_d}{\partial R} R \, d\alpha$$

$$= \int_{\pi/2}^{-\pi/2} \left(\phi \Big|_d + R \cos\alpha \frac{\partial \phi}{\partial n} \Big|_d - R \sin\alpha \frac{\partial \phi}{\partial s} \Big|_d \right) \left(\frac{-\sin\alpha}{R^2} \right) R \, d\alpha$$

$$= + \frac{\pi}{2} \frac{\partial \phi}{\partial s} \Big|_d \quad . \qquad .$$

The closing segment of the contour from the free surface to the ⊄ of symmetry on the infinite boundary is represented by

$$\int_{s=\infty}^{⊄=\infty} \quad .$$

Even though this integral is over an infinite boundary, it is definitely zero because ϕ, ϕ_d, $\partial\phi/\partial n$, and $\partial\phi_d/\partial n$ are zero on the infinite boundary.

Now that the integral for each segment of the contour has been reviewed, it is simple to write the integral Equation (24)

$$\oint_s \phi_d \frac{\partial \phi}{\partial n} ds = \oint_s \phi \frac{\partial \phi_d}{\partial n} ds$$

which may be broken down into sections according to the discussion above to give:

$$2 \, V \mu \cos\beta + \int_{o'}^{\infty} \phi_d \frac{\partial \phi}{\partial n} ds - \frac{\pi}{2} \frac{\partial \phi}{\partial s} \Big|_d = \int_o^{\infty} \phi \frac{\partial \phi_d}{\partial n} ds + \frac{\pi}{2} \frac{\partial \phi}{\partial s} \Big|_d \quad . \tag{30}$$

This reduces to:

$$-\pi \frac{\partial \phi}{\partial s} \Big|_d + 2 \, V \mu \cos\beta = \int_{o'}^{\infty} \left(\phi \frac{\partial \phi_d}{\partial n} - \phi_d \frac{\partial \phi}{\partial n} \right) ds \quad . \tag{31}$$

Equation (31) expresses the condition of irrotationality in a form which may be applied to the trial curves which have been obtained from the first two conditions. By trial-and-error solution, the final shape of the fluid surface which will satisfy the third and final condition may be found for each wedge angle.

DETERMINATION OF LOADS AND PRESSURES

From the above portion of the analysis, the shape of the free surface for potential flow due to the constant-velocity immersion of a wedge has been determined. The values of velocity, potential, and stream function on the free surface corresponding to this shape are directly ob-

tained, as indicated previously. However, (in order to obtain the pressure on the wedge) velocity and potential values along the wedge surface are required, and these are not directly given by the analysis so far. The study will be extended to yield this information, but first, the method of obtaining the total load as proposed by Wagner (Reference 8) will be developed.

WAGNER'S METHOD FOR TOTAL LOAD

Penetration of the wedge into the fluid generates pressures on the wedge which appear in the fluid flow as momentum and kinetic energy (under the initial assumptions of the perfect fluid without restraining boundaries). The total force at any time equals the rate of change of momentum, and the work done by the force is equivalent to the kinetic energy of the fluid.

The momentum of the fluid, M, is given by summation of the products of incremental volume, $d(vol)$, and the local velocity vector, $\nabla\phi = grad\phi$:

$$M = \rho \iiint \nabla \phi \, d(vol) \quad .$$

Since the local velocity, $\nabla\phi$, at any position is constant for a constant velocity penetration, the change in momentum with respect to time at a given position in the fluid is given by the rate of increase of the differential volume. For the two-dimensional case under consideration, the differential volume, $d(vol)$, to occupy a given space increases directly as the area of immersion, or directly as the square of the depth of immersion. Thus, $d(vol) \approx A \approx y_0^2 \approx t^2$.

The total force is then given by

$$P = \frac{dM}{dt} = \rho \frac{d}{dt} \iiint t^2 \, \nabla \phi \, \frac{d(vol)}{t^2} \quad ,$$

where $\nabla\phi$ and $d(vol)/t^2$ are for relative positions and independent of time t. The differential of the integral with respect to time gives

$$P = \frac{2\rho}{t} \iiint \nabla \phi \, d(vol) \quad . \tag{32}$$

This integral can be transformed to a surface integral by the theorem of divergence (Gauss' theorem)

$$\iiint \nabla \phi \, d(vol) = - \iint \phi \, df \, ,$$

where the differential area, df, is a vector normal to the surface, positive inward with respect to the surface. Substitution in Equation (32) gives

$$P_t = -2\rho \iint \phi \, df \quad , \tag{33}$$

which for the two-dimensional case under consideration may be written:

$$P_t = -2\rho \int \phi \, ds \ ,$$

where P represents the load per unit length of the infinite wedge.

Because of the symmetry of the problem, the horizontal components of the vector, $\phi \, df$, balance. Thus, only the vertical components need be integrated to obtain the load P (which must obviously be normal to the initial fluid surface for the symmetrical problem under consideration). The vertical components of the incremental vectors, $\phi \, ds$, may be written as $\phi \, dx$, where dx is the horizontal projection of an elemental surface length. The direction (up or down) of $\phi \, dx$ is determined by the sign of the quantity dx, depending upon the position of the surface with respect to the fluid, as shown in Figure 6. Along the wedge, $dx = \cos\beta \, ds$ and the vertical component of $\phi \, ds = \cos\beta \, \phi \, ds$. On the spray surface the inward vector is upwardly inclined so that $ds \approx -dx$, while on the wave surface the inward normal is downward so that $ds \approx dx$.

Now, if V_n represents the component of the field velocity, V, normal to the surface and positive inwards, V_n will be negative in the spray and positive in the wave area as shown in Figure 6. Thus, in both regions, dx may be written as

$$dx = \frac{V_n}{V} ds$$

and the vertical component of $\phi \, df$ is

$$\phi \, dx = \phi \frac{V_n}{V} ds \quad .$$

The integral for total load, Equation (33), may then be written in two parts: one for the body, S_B, and one for the free surface, S_W:

$$P_t = -2\rho \int_S \phi \, ds = -2\rho \int_S \phi \, dx$$

and

$$P_t = -2\rho \cos\beta \int_{S_B} \phi \, ds \ -2\rho \int_{S_W} \phi \frac{V_n}{V} ds \ . \tag{34}$$

The kinetic energy, K.E., of the fluid field is given by Greene's theorem in terms of a surface integral (Reference 9):

$$\mathrm{K.E.} = \rho \iiint \left(\frac{\phi_x^2}{2} + \frac{\phi_y^2}{2} \right) d(\mathrm{vol}) = -\frac{\rho}{2} \iint \phi \frac{\partial \phi}{\partial n} df, \tag{35}$$

where positive energy is indicated by flow outward through the surface, $-\partial\phi/\partial n$. The kinetic energy per unit thickness of the wedge is therefore

$$K.E. = -\frac{\rho}{2}\int \phi \frac{\partial \phi}{\partial n}\,ds \quad .$$

By virtue of the uniform growth of the loaded area for the simple wedge immersing at constant velocity, the load on the wedge increases linearly with time. (This may also be deduced, mathematically, from Equation (32).) Thus $P = (P/t)t$, and the work done is given by the integral of the load, P, times the distance, dy ($= V\,dt$):

$$\text{Work} = \int P\,dy = \int \left(\frac{P}{t}\right) t\; V\,dt = \left(\frac{P}{t}\right) V \frac{t^2}{2} = \frac{PVt}{2} \quad .$$

Since the work done on the perfect fluid must equal the change in kinetic energy,

$$\frac{PVt}{2} = K.E. = -\frac{\rho}{2}\int_S \phi \frac{\partial \phi}{\partial n}\,ds \quad . \tag{36}$$

Since, at the body, $\partial \phi/\partial n = +\,V \cos\beta$, and on the free surface, $\partial\phi/\partial n$ is negative, variable with position, Equation (36) may be written:

$$\frac{PVt}{2} = -\frac{\rho}{2}\left(+\,V \cos\beta \int_{S_B} \phi\,ds + \int_{S_V} \phi \frac{\partial \phi}{\partial n}\,ds\right)$$

or

$$Pt = -\rho \cos\beta \int_{S_B} \phi\,ds - \frac{\rho}{V}\int_{S_V} \phi \frac{\partial \phi}{\partial n}\,ds \quad . \tag{37}$$

It will be noted that both Equations (34) and (37) contain a term which requires values of the potential on the body for solution. However, they may be solved simultaneously to yield a solution for the load P in terms of the free surface integrals alone, eliminating the troublesome term.

Equation (34) minus twice Equation (37) gives:

$$Pt - 2\,Pt = -2\rho \int_{S_V} \phi \frac{V_n}{V}\,ds + \frac{2\rho}{V}\int_{S_V} \phi \frac{\partial \phi}{\partial n}\,ds$$

$$-PVt = 2\rho\left(\int_{S_V} \phi \frac{\partial \phi}{\partial n}\,ds - \int_{S_V} \phi\,V_n\,ds\right)$$

$$-PVt = 2\rho \int_{S_V} \phi \left(-V_n + \frac{\partial \phi}{\partial n}\right)ds \quad . \tag{38}$$

This integral may be evaluated for each deadrise investigated since the required potential and normal velocities are given at every point on the free surface. In general, the velocity and potential have been ob-

tained in terms of distances in the geometric construction $(tV, t\phi)$. Equation (38) may be converted to this form by multiplication by t^2:

$$PVt^3 = -2\rho \int_{S_{\sy}} t\phi \left(-tV_n + t \frac{\partial\phi}{\partial n} \right) ds$$

or since $y_o = tV$,

$$\frac{P}{\frac{\rho}{2}V^2} = \frac{4}{y_o^3} \int_{S_{\sy}} t\phi \left(tV_n - t \frac{\partial\phi}{\partial n} \right) ds \ . \tag{39}$$

Equation (39) is the final form for convenient evaluation of the load on the immersing wedge in terms of the free surface shape determined in the previous section.

It may be seen by reference to Equation (20) and Figure 3 that the major portion of this integral accrues in the spray region. The value of potential is large at the spray tip and decreases rapidly to low values past the spray root, while the relative normal velocity component increases to a much smaller extent in the spray-root region. The product of potential and normal velocity diminishes rapidly to zero along the wave surface towards infinity because, while the velocity approaches a constant value $[tV_n - t(\partial\phi/\partial n) = tV]$, the product $t\phi$ diminishes as the distance squared.

Closer scrutiny of the relative velocity $[V_n - (\partial\phi/\partial n)]$ shows the direct relationship between the spray thickness and the total force according to Equation (38). The velocity $[V_n - (\partial\phi/\partial n)]$ is actually the normal component of the vector sum of V and U_c in Figure 3. In the spray region, this is practically constant and equal to the velocity of the spray tip along the wedge times the angle between spray and wedge. Thus, the thickness of spray determines the relative normal component in the region in which the greatest part of the force integral is determined, and so the force is roughly proportional to the spray thickness.

DERIVATION OF POTENTIAL AND VELOCITY DISTRIBUTIONS ON THE WEDGE SURFACE

From the simple graphical constructions described in the previous section, the analysis of the free surface shape for any wedge angle will give directly the velocity and potential distributions on the free surface. Also, a method has been given for obtaining the total load on the wedge, which circumvents the necessity for detailed flow information along the wedge itself. However, the distribution of the pressure on the wedge has not been given, and for that purpose the potential and velocity distributions on the wedge surface are required.

On the premise that the unique free surface shape for each wedge is a result of potential flow, the velocity and potential at any point may be represented by complex analytic functions:

$$U = \frac{dw}{dz} = u - iv$$

$$w = \phi + i\psi$$

to which the Cauchy integral equation may be applied, relating the point value of a function to the integral around a bounding contour of values of the function at other points. The standard integral for the point within the boundary is·

$$f(z_o) = \frac{1}{2\pi i} \oint_c \frac{f(z)}{z - z_o} \, dz \quad , \tag{40}$$

where z is the complex coordinate of the position in the field. Since points on the solid boundary are to be investigated, the bounding contour circles only halfway around the point in passing so that the factor 2π is reduced to π, and the principal value of the integral is used. Thus, for the velocity $U = u_\beta - iv_\beta = f(z)$:

$$U(z_o) = \frac{1}{\pi i} \oint_c \frac{U(z)}{z - z_o} \, dz \quad . \tag{41}$$

This equation may be separated into real and imaginary parts by placing the origin of coordinates, $z_\beta = x_\beta + iy_\beta$, at the point z_o being investigated, and writing z in the polar form:

$$z = \rho e^{i\theta} = e^{\ln\rho + i\theta} \tag{42}$$

$$dz = e^{\ln\rho + i\theta} [d(\ln \rho) + i \, d\theta] = z \, [d(\ln \rho) + i \, d\theta] \quad . \tag{43}$$

Substitution of these expressions for z and dz into Equation (41) gives

$$U(z_o) = u_{o_\beta} - iv_{o_\beta} = \frac{1}{\pi i} \oint_c [u_\beta - iv_\beta][d(\ln \rho) + i \, d\theta] \quad . \tag{44}$$

Rearranging the terms gives

$$i\pi u_{o_\beta} + \pi v_{o_\beta} = \oint_c u_\beta \, d(\ln\rho) + v_\beta \, d\theta + i \, [u_\beta d\theta - v_\beta \, d(\ln \rho)] \quad ,$$

so that the real and imaginary parts of $U(z_o)$ may be separated:

$$v_{o_\beta} = \frac{1}{\pi} \oint_c v_\beta \, d\theta + u_\beta \, d(\ln \rho) \tag{45a}$$

$$u_{o_\beta} = \frac{1}{\pi} \oint_c u_\beta \, d\theta - v_\beta \, d(\ln \rho) \quad . \tag{45b}$$

The construction for performing this integration is shown in Figure 7. The complex coordinates are taken with the iy_β axis along the wedge, positive towards the spray tip. The x_β axis is then normal to the wedge surface, positive into the fluid. The axes are so chosen that the integral for v_β need not be evaluated along one side of the wedge since u_β is constant ($= V\cos\beta$) and $d\theta = 0$ (except for the infinitesimal region of the singularity). On the far side of the wedge, the value of v_β must be estimated until the first solutions for v_β are obtained. However, these points are sufficiently distant to have small effect, and a rapidly convergent solution is obtained.

The potential on the wedge surface may be obtained by integrating the velocity along the wedge from the spray tip (where the free surface formula, Equation (20), gives the coincident value) to the apex of the wedge. The potential may also be found directly by the integral relation corresponding to Equation (45) (ϕ in place of u_β, and ψ in place of $-v_\beta$). This is more laborious, and only a few points need be investigated to check the results from the velocity integration along the surface of the wedge.

PRESSURE DISTRIBUTION

The velocity distribution and potential along both the free surface and the immersed portion of the wedge have been determined in the previous sections. It now remains to compute the pressures which correspond to this potential flow.

As was noted before, particles in the fluid move relative to the shape of the flow field (across instantaneous streamlines). Thus, the simple Bernoulli pressure equation may not be used since particular streamlines exist only instantaneously, even though the flow pattern is always similar. For this problem, the general equation for fluid pressure in a potential flow must be used (Reference 9):

$$\frac{P}{\rho} - \frac{\partial\phi}{\partial t} - \frac{U^2}{2} + F(t) + \Omega \quad . \tag{46}$$

Since the fluid has been assumed to be at rest at infinity, with gravity neglected, the gravitational field and extraneous impulses, represented by Ω and $F(t)$, are zero. The resultant field velocity, U, has been determined on the free surface, (Equation (15)), and on the wedge (Equation (45)). The rate of change of potential with time, $\partial\phi/\partial t$, may be determined as follows.

At any position r/y_0 in the fluid (see Figure 8), the potential ϕ is a linear function of time (since time is directly related to the scale, or size, of the symmetrical, constant-velocity penetration under consideration):

$$\phi_{r_t} = \phi_{r_{t_1}} \frac{t}{t_1} \quad . \tag{47}$$

However, at a fixed point (x,y) in the field, this is not so. Consider the point (x,y) to coincide with the position r_{t_1}/y_0 at t_1. At $t = t_1 + \Delta t$, the position r_t/y_0 is a distance $\Delta r = r\Delta t/t$ from (x,y). (For small Δt, the velocity U in the region may be assumed constant in magnitude and direction.)

Then, at $t = t_1$,

$$\phi_{(x,y)_{t_1}} = \phi_{r_{t_1}} \quad ;$$

at $t = t_1 + \Delta t$,

$$\phi_{(x,y)_{t_1+\Delta t}} = \phi_{r_t} - U \cos\alpha \, \Delta r \ ,$$

where $U \cos\alpha$ is the component of the velocity along r. Thus,

$$\Delta\phi = \phi_{(x,y)_{t_1+\Delta t}} - \phi_{(x,y)_{t_1}} = \phi_{r_t} - U \Delta r \cos\alpha - \phi_{r_{t_1}} \ . \tag{48}$$

With $t = t_1 + \Delta t$, from Equation (47),

$$\phi_{r_t} = \phi_{r_{t_1}} \frac{t_1 + \Delta t}{t_1} = \phi_{r_{t_1}} + \frac{\Delta t}{t_1} \phi_{r_{t_1}} \ .$$

Equation (48) then reduces to

$$\Delta\phi = +\frac{\Delta t}{t_1} \phi_{r_{t_1}} - U \Delta r \cos\alpha \quad . \tag{49}$$

The partial derivative $\partial\phi/\partial t$ is obtained from the limit of Equation (49) as Δt approaches 0:

$$\frac{\partial\phi}{\partial t} = \lim_{\Delta t \to 0} \frac{\Delta\phi}{\Delta t} = \lim_{\Delta t \to 0} \left(+\frac{\phi_{r_{t_1}}}{t_1} - \frac{\Delta r}{\Delta t} U \cos\alpha \right)$$

$$= +\frac{\phi}{t} - \frac{r}{t} U \cos\alpha \quad . \tag{50}$$

where the subscripts are no longer needed since the analysis applies to all points in the fluid. The pressure distribution is then determined by

$$\frac{P}{\rho} = -\frac{\phi}{t} + \frac{r}{t} U \cos\alpha - \frac{U^2}{2} \ , \tag{51}$$

where the expression for $\partial\phi/\partial t$ from Equation (50) has been substituted in Equation (46) (with $\Omega = F(t) = 0$).

On the free surface. the pressure should be zero. This may be checked by referring back to the geometric relations between the velocities and potential shown in Figure 3 and Equation (21). These values substituted in Equation (53) yield

$$\frac{P}{\rho} = \frac{U_s^2}{2} - \frac{U_r^2}{2} + U\,U_r\,\cos\alpha - \frac{U^2}{2} \quad,$$

the right-hand side of which will be recognized to be zero from the solution for a triangle side U_s in terms of U_r, U, and the included angle, α.

On the wedge, the pressure may be found by substituting the values of r, ϕ, U, and α determined previously. The total load on the wedge is obtained from the integration of the edge pressure across the projected wetted width. This value may then be compared with that obtained on the basis of Wagner's analysis for the integral over the free surface only (Equation (39)).

Maximum-pressure location and magnitude along the wedge may be found by setting equal to zero the first derivative with respect to s of Equation (51):

$$\frac{dP}{ds} = \frac{1}{t}\frac{d\phi}{ds} + \frac{1}{t}\,U\,\cos\alpha\,\frac{dr}{ds} + \frac{r}{t}\,\cos\alpha\,\frac{dU}{ds} - U\,\frac{dU}{ds} = 0.$$

Now $U\cos\alpha = d\phi/dr$ so that at P_{max} (or P_{min}),

$$\frac{r}{t}\cos\alpha\frac{dU}{ds} = U\frac{dU}{ds} \quad. \tag{52}$$

A maximum or minimum can occur when $dU/ds = 0$ or when $r/t = U/\cos\alpha$. Since the former occurs at the spray tip, a minimum pressure point, it may be ignored. Substitution of the latter into Equation (51) gives

$$\frac{P_{max}}{\rho} = -\frac{\phi}{t} + \frac{U^2}{2} \quad, \tag{53}$$

or in terms of r,

$$\frac{P_{max}}{\rho} = -\frac{\phi}{t} + \frac{r^2\cos^2\alpha}{2t^2} \quad. \tag{54}$$

Further study of the relationship $r/t = U/\cos\alpha$ shows that at this

point, α must be zero. This follows from the observation that the component of U at the wedge normal to the wedge is constant and equal to the component of r/t normal to the wedge. Thus, r/t can equal $U/\cos\alpha$ only when $r/t = U$ and $\alpha = 0°$. Dividing both sides of Equation (54) by $V^2/2 = y^2/2t^2$ and putting $\cos\alpha = 1$, gives

$$\frac{P_{max}}{\rho V^2/2} = -\frac{2\phi t}{y_o^2} + \frac{r^2}{y_o^2} = -\frac{2\phi t}{y_o^2} + \frac{U^2}{V^2} \tag{55}$$

at the point (or points) where $r/t = U$.

It is interesting to note that the peak pressure point $r/t = U$ corresponds to a stagnation point in that the same particle occupies the same relative position at all times. However, the pressure is not the simple relation $\rho U^2/2$, but is greater or less depending on whether the potential at the point is less or greater than 0.

RESULTS OF ANALYSIS AND COMPARISONS WITH OTHER METHODS

SURFACE SHAPE

The details of computation and drafting required for the application of the continuity, similarity, and irrotationality conditions to the penetration of a 40° deadrise angle wedge are given in Appendix I. Similar calculations were performed for angles of 20°[*], 30°, and 50°. The final surface shape determined by the iterative solution is shown for each angle in Figure 9.

The spray thickness appears to be the most critical characteristic for a quantitative description of each surface. However, since the spray is tapered to a point at its edge and merges into the spray-root region, it is necessary to establish a consistent definition for the spray thickness. It was noted that in every case the spray root comes quite close to the nominal half-width, c. Therefore, this nominal width was used as a reference line, and the spray thickness was defined as the distance from the wedge surface to the intersection of the straight portion of the spray surface extended to the half-width, c, as shown in Figure 9. The ratio of spray thickness to half-width, δ/c, defines the relative spray for each wedge angle. The three surfaces computed in detail were used as the basis for the plot of relative spray thickness vs. wedge angle given in Figure 10. The points are approximately fitted by the formula

$$\frac{\delta}{c} = \frac{\sin\beta \tan\beta}{3.3\pi} \tag{56}$$

---

[*] The spray thickness for $\beta = 20°$ was taken from the curve determined by the other three, and only continuity and similarity conditions were applied.

In References 3 and 8, an analytical solution is obtained for the flow in the region of an immersing wedge by comparison with the solution for the flow around an expanding flat plate. This solution gives an expression for the rise of the free water surface (Equation (3)), with no spray.

The mathematical analysis of the spray-root region (References 2 and 8) describes the flow in the immediate area of the spray root, but the boundaries of the problem are doubly infinite and do not correspond to the conditions of the penetrating wedge. The flow is defined in terms of the spray thickness which is not readily determined for the finite problem.

Wagner obtained an approximate expression for the spray thickness by comparing the flow fields at infinity for the spray-root and expanding-plate analyses (Reference 8, Equation 47):

$$\frac{\delta}{c} = \frac{\pi}{8} u^2 \quad ,$$

where $u = 2 \tan\beta/\pi$, and therefore,

$$\frac{\delta}{c} = \frac{\tan^2\beta}{2\pi} \quad . \tag{57}$$

However, the logical procedure by which this formula was obtained is not readily apparent in the referenced report. Later, unpublished work by Wagner indicated that a factor of 0.7 (approximately) should be applied to the spray thickness obtained from Equation (57).

A more reasonable comparison of the spray-root and expanding-plate analyses may be made in the region of the spray root itself. This comparison is based upon the assumption that the stagnation point of the spray-root analysis will occur at the peak-pressure point for the expanding-plate analysis. A superposition of the two flows with the 'stagnation' as a common point is shown in Figure 11.

In the previous analysis of spray-root flow (Reference 2), the scale was indeterminate and the local region was not related to the overall picture of a wedge-penetration problem. The distance A in Figure 11 is approximately equal to the distance from spray root to stagnation point of the previous analysis, and may be obtained in terms of the spray thickness, δ, from Figure 6 of Reference 2 by projection of the root into the $x\pi/\delta$ axis (at a value of 6). For the angles investigated, $A \cong 6\pi/\delta$ and

$$c - \bar{x} = (\delta \tan\beta + A) \cos\beta = \delta (\sin\beta + \frac{6}{\pi} \cos\beta) \quad . \tag{58}$$

The expanding-plate analogy mentioned previously does not give a practical physical solution because of the absence of spray, but by that

method of analysis, a definite relationship is established between the wedge angle and the stagnation point. Now $\bar{x}/c$ is given by Equation 30 of Reference 3 as

$$\frac{\bar{x}}{c} = \sqrt{1 - \lambda^2} = \sqrt{1 - (2 \tan\beta/\pi)^2} \, ,$$

and substitution of this value from the expanding-plate analogy into Equation (58) relates the spray thickness ratio δ/c to the wedge angle, β:

$$c - c \sqrt{1 - (2 \tan\beta/\pi)^2} = \delta \left(\sin\beta + \frac{6}{\pi} \cos\beta\right)$$

$$\frac{\delta}{c} = \frac{1 - \sqrt{1 - (2 \tan\beta/\pi)^2}}{\sin\beta + \frac{6}{\pi} \cos\beta} \, . \tag{59}$$

Equations (57) and (59) are plotted in Figure 10 for comparison with the points determined by the present analysis. It will be noted that the three points computed in detail (at 30°, 40°, and 50° deadrise) approach the curve of Equation (59) at the lower angles. Also, Equation (59) approaches 70% of Equation (57) at low deadrise angles.

VELOCITY POTENTIAL, AND STREAM FUNCTION

Under the conditions for irrotational flow of a perfect fluid, the shape of the free surface has been determined for several wedge angles. In fact, the solution for the surface shape is the key to the field of flow everywhere in the fluid. The values of the velocity, potential, and stream function on the free surface are given directly, while the values on the wedge must be estimated and then refined by an iterative solution.

FREE SURFACE

Velocity and potential at the free surface are given by Equations (15) and (21) respectively. These have already been computed for the several stages of the solution for the free surface shape. The final set of values for each wedge angle are plotted in Figures 12, 13, and 14 as U/V, α, and $\phi t/c^2$ respectively vs. position on the surface, s/c. The stream function is given on the free surface by Equation (22). The values of $\psi t/c^2$ vs. s/c for the several wedge angles are plotted in Figure 15.

SOLID BOUNDARY

At the wedge, the normal component of the velocity, u_β, is constant ($V \cos\beta$), and the stream function is given directly by

$$\psi = sV \cos\beta + \widehat{y_0 o}' \ V \cos\beta,$$

where s, the distance from the spray tip, will be negative along the wedge. The tangential component of the velocity at the wedge, v_β, must be estimated so that the complete integral, Equation (45), may be evaluated. The revised values obtained from the iterated solution of the Cauchy integral for each wedge angle are plotted in Figure 16. These data are combined with the constant u_β and shown in Figures 12 and 13.

Values of the potential on the wedge were obtained from the integration of the velocity distribution from wedge apex to spray tip and vice versa. The end points for the potential (at spray tip and wedge apex) were obtained from Equation (21) and the potential relationship corresponding to Equation (45). Since the mechanical work involved in the construction practically precludes a perfect agreement, the curves of $\phi t/c^2$ vs. s/c along the wedge presented in Figure 14 represent average values obtained by working from either end toward the center of the wedge side.

It is of interest to compare the potential and velocity from the present analysis with those for the immersing wedge as given by the expanding-plate analogy. Equation 4 of Reference 3 gives for the potential on the plate

$$\phi = -V\sqrt{c^2 - x^2}$$

or

$$\frac{\phi t}{c^2} = -\frac{Vt}{c}\sqrt{1 - \left(\frac{x}{c}\right)^2} \qquad .$$

This expression is indicated by the dotted lines in Figure 14 (with signs reversed for clarity).

Equation 5 of Reference 3 gives for the velocity along the plate

$$v_\beta = U = V\frac{x}{\sqrt{c^2 - x^2}}$$

or

$$tv_\beta = \frac{tV}{\sqrt{(c/x)^2 - 1}} \qquad .$$

This expression is represented by the dotted lines in Figure 16.

It will be noted that the velocity and potential distributions along the wedge obtained by the earlier method (Reference 3) are in partial agreement at the lower angles, but that the results of the two methods diverge at higher angles.

PRESSURES AND LOADS

The pressure distribution on the wedge surface is given by Equation (51). The values of $\phi t/c^2$, U/V, and α have been calculated already and are plotted in Figures 14, 12, and 13, while r/Vt may be measured directly. The computed pressures for the 20°, 30°, 40°, and 50° deadrise wedges are plotted in Figure 17.

Total load on the wedge may be obtained by integrating the pressure distribution along the bottom. Because of the symmetry of the wedge, only the vertical component need be taken since the lateral forces from the two sides will cancel each other. Thus, for the complete wedge (two sides):

$$P = 2 \cos\beta \int_{y_o}^{o'} p \, ds$$

and

$$\frac{P}{c(\rho V^2/2)} = \frac{2 \cos\beta}{c} \int_{y_c}^{o'} \frac{p}{\rho V^2/2} \, ds \quad .$$

The loads obtained by integrating the pressures for the three wedges investigated have been used to construct the curve of $P/c(\rho V^2/2)$ vs. β given in Figure 18.

For comparison with Wagner's analysis of the total load, the values of $P/c(\rho V^2/2)$ obtained by Equation (39) are also shown in Figure 18. The functions in Equation (39) to be integrated are plotted in Figure 19 for each wedge angle.

The earlier analysis (Reference 3) of the immersing wedge was shown to be in agreement with experimental data at deadrise angles of approximately 20°. For comparison with the present, more detailed analysis, the pressure distributions and loads from the expanding-plate analogy have been computed and are plotted in Figures 17 and 18 (according to Equation 46 of Reference 3) for 20°, 30°, 40°, and 50° deadrise.

In Equation 76 of Reference 8, the solution for total load on an 18° wedge was given as:

$$P = 49 \ 8 \ T \ \rho \ V^2 \quad ,$$

where T is equivalent, in the notation of this report, to $V = (2c/\pi)\tan\beta$. Then,

$$\frac{P}{c(\rho V^2/2)} = 49.8 \times \frac{2}{\pi} \tan 18^\circ \times 2 = 20.7 \text{ (two sides)}$$

This value for $\beta = 18^\circ$ is indicated in Figure 18, along with Wagner's approximation for the variation of load with deadrise (Equation 78 of Reference 8),

$$\frac{P}{c(\rho V^2/2)} = 2 \tan\beta \left(\frac{90^\circ}{\beta} - 1\right)^2 \qquad .$$

Comparison of the various load results shown in Figure 18 indicates several noteworthy trends. As was to be expected (within the accuracy of the drafting and computation required), the loads obtained by the present analysis are in reasonable agreement whether obtained by Wagner's method or by integration of the bottom pressures. The expanding-plate analogy indicates higher pressures and loads than the present analysis, with the percentage difference increasing with deadrise angle up to 50°. The single point for load at $\beta = 18^\circ$ given in Reference 8 lies far below the curve obtained on the basis of the expanding-plate analogy (Reference 3). This point and Wagner's approximate curve lie about 8% below an extension of the curve of loads determined by the present analysis.

Thus, the variation of load with deadrise angle, as determined by the integration of the bottom pressure, may be approximated by

$$\frac{P}{c(\rho V^2/2)} = 2.16 \tan\beta \left(\frac{90^\circ}{\beta} - 1\right)^2 \qquad .$$

DISCUSSION

SURFACE SHAPE

The theoretical analysis for the determination of the spray thickness was concluded with a method for checking the irrotationality of the flow field, using an artifice involving the superposition of a known flow (doublet) and the graphical application of Greene's theorem (Equation (31)). In spite of the great care taken in drafting and computation details, the spray thickness could not be established as precisely as desired. The curve presented in Figure 10 was selected as representative of the computed points, even though the relative position of the 30° and 40° points indicate a possible flexure in the curve.

After the determination of the loads and pressures, another check on the spray thickness became apparent. Wagner's analysis for the total load based upon a simultaneous solution of momentum and kinetic energy

relationships holds only for irrotational potential flow. It was noted previously that the load was almost directly proportional to the spray thickness. Also, it appeared from the actual calculations that the velocity and potential distributions were affected only slightly by the value of the spray thickness. Thus, the agreement between the results of the earlier load analysis (Equation (39)) with the integration of the pressures on the wedge is a measure of the accuracy of the spray thickness.

Application of this criterion to the results given in Figure 18 indicates that the spray thicknesses for 40° and 50° deadrise are too large, while at 20°, the estimated spray must have been too thin. If the load analyses are assumed to be accurate, then the revisions in spray thicknesses required to give consistent force results are proportional to the difference between the computed load points. A revised set of spray thickness points was determined in this manner and plotted in Figure 10. These revised values of the spray thickness are very well fitted by

$$\frac{\delta}{c} = \left(\frac{\beta}{\pi}\right)^2 \qquad (60)$$

It should be noted that the spray thickness is of a small order of magnitude. At 20° deadrise, the total thickness is only slightly more than 1% of the wetted half-width, while at the highest angle investigated, the spray thickness ratio is only 8%. (This factor will make experimental verification of the surface shape very difficult except in a qualitative way.) In view of the amount of graphical construction involved in the present analysis, the spread between the spray thickness curves in Figure 10 is not unreasonable.

If extension of the computations to higher deadrise angles becomes desirable, it will probably be sufficient to by-pass the doublet check on irrotationality and go directly to the determination of loads and pressures for surface curves based on the extrapolated values of δ/c from Equation (60). Since the computation of loads and pressures is not too tedious for the estimated spray thickness and surface shape, and since the approximate correction to the spray may be estimated using the approximate proportionality between the load and spray thickness, it would be economical to use the load integrals as the check on the irrotationality of the flow field.
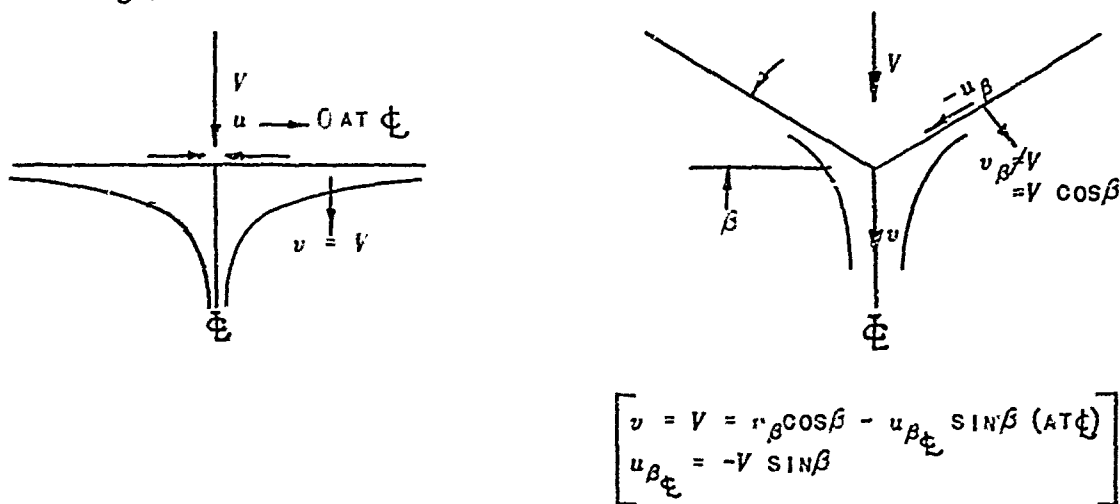
The emphasis in this discussion has been upon the determination of the relative spray thickness. This is so because the shape of the surface may be very closely approximated by the graphical construction method for similiarity and continuity once the proper spray thickness is known.

VELOCITY AND POTENTIAL DISTRIBUTIONS ALONG THE WEDGE

It has been noted that the velocity along the wedge as determined from this analysis is in partial agreement with that indicated by the expanding-plate analysis. As discussed in Reference 3, the plate analogy

breaks down near the edge with the indication of infinite velocity. That would be a physical impossibility, and in actuality, a spray root is formed. The velocity increases less rapidly than indicated by the expanding-plate analysis, as indicated in Figure 16, and then levels off to a constant value in the spray.

By virtue of the symmetry, at the centerline of a flat expanding plate the velocity along the plate must be zero. However, on the actual wedge, there is a component along the wedge toward the center so that the resultant velocity at the apex is vertical (not normal to the bottom of the wedge).

$$\begin{bmatrix} v = V = v_\beta \cos\beta - u_{\beta_\mathbb{C}} \sin\beta \ (\text{AT}\ \mathbb{C}) \\ u_{\beta_\mathbb{C}} = -V \sin\beta \end{bmatrix}$$

This is the difference which appears at $x/c = 0$ in Figure 16. The close agreement between the velocity curves in the range $0.4 < x/c < 0.95$ is quite remarkable, expecially for the $30°$ deadrise wedge. The increase with increasing deadrise in the difference between the present curves and those from the expanding-plate analogy appears to be due primarily to the condition at the step apex discussed above.

With respect to the potential on the wedge as given by the present analysis compared to that from the expanding-plate analogy, a more involved reasoning is required. It will be noted in Figure 14 that the previous and present analyses give the same shape of potential distribution, but that the expanding-plate analogy indicates higher negative values (almost a constant difference along s/c for any particular deadrise angle). Under the assumptions of Reference 3 (expanding-plate analogy), the potential is based at zero on the level of the plate. This becomes an untenable position at any appreciable deadrise angle, since the level water surface lies above the wedge apex, and the plate cannot be construed as being at several levels simultaneously. The difference in potential of the field for a reference-level change of y_o $[=(2c/\pi)\tan\beta]$ is Vy_o. In terms of the scale on Figure 14, the change in $\phi t/c^2$ is

$$\Delta \frac{\phi t}{c^2} = \frac{tVy_o}{c^2} = \frac{y_o^2}{c^2} = \frac{4\tan^2\beta}{\pi^2}$$

This is almost exactly the difference at the lower deadrise angles between the expanding-plate potential and the distribution given by the present, more exact analysis.

PRESSURES AND LOADS

Because of the independent check of the spray thickness by the comparison of total load and integrated pressure distributions, it may be reasoned that the pressures are reasonably accurate. This could not be assumed to be the case if such a check had not been obtained. because of the number of terms and graphical constructions involved in the steps leading to the determination of the pressure.

The failure of the expanding-plate analogy in predicting the correct wedge pressures may be partly due to the difference in potential which was discussed above. It may be shown (by reference to Equation (51)) that a change in potential ($\Delta\phi = Vy_o$) shows up in the pressure ratio, $P/(\rho V^2/2)$, as an additive term (of value -2). Thus, a changed potential reference in the expanding-plate analogy will reduce the pressures shown in Figure 17 by 2. This does not bring all of the curves into alignment, but a trend in that direction is obviously correct.

It may be seen in Figure 17 that the trends of the pressure differences at the peak (in the spray root) and at the keel are opposite. Although the expanding-plate maximum pressures are higher than those obtained from the present detailed analysis, the percentage excess decreases with decreasing deadrise. On the other hand, the keel pressure given by the earlier analysis is higher at low deadrise angles (approximately by the amount of 2, as mentioned above), but the difference decreases with increasing angle.

It is interesting to note that a rather uniform pressure distribution is obtained at 40° deadrise angle. At lower angles, the peak pressures greatly exceed the average value across the section, while at higher angles, the lack of a well-defined stagnation area in the spray-root region lets the pressure drop below the value at the keel. This trend had been shown before in the expanding-plate analysis, but could not be accepted upon that basis alone because of the wide divergence from the conditions assumed for that analysis. However, the removal of the restriction to low angles made possible by the present analysis has resulted in a similar variation of pressure with deadrise angle, so that the trend may be considered to be established.

CONCLUSIONS

1. A method has been presented for the theoretical determination of the free surface shape arising from the symmetrical penetration of the surface of a perfect fluid by an infinite wedge-shaped body at constant

velocity (normal to the initial undisturbed surface)

2. The actual surface shapes have been constructed for 20°, 30°, 40°, and 50° deadrise angles.

3. Since no restriction upon the wedge angle or slope of the free surface was necessary to this solution, the method may be used for even greater deadrise angles when desirable.

4 In the process for constructing these surface shapes, the spray thickness ratio appeared as the most critical dimension. The spray is uniformly tapered from zero thickness at the tip to a maximum in the spray root where it is related to the wetted half-width by the empirical relationship $\delta/c = (\beta/\pi)^2$.

5. Distributions of the velocity, potential, and pressure along the wedge surface were evaluated by the extension of the solution for the free surface shape These distributions are similar to those given by the earlier expanding-plate analysis (Reference 3) except that an accurate description of the flow is now given in the spray-root region.

6 The total loads, obtained by the integration of the pressure over the wetted width of the wedge, are given by the empirical relationship

$$\frac{P}{c(\rho V^2/2)} = 2.16 \ \tan\beta\left(\frac{\pi}{2\beta} - 1\right)^2 \qquad ,$$

which is 8% higher than Wagner's approximation of the same form.

REFERENCES

1 Korvin-Kroukovsky, B V and Chabrow, Faye R. *The Discontinuous Fluid Flow Past an Immersed Wedge.* Stevens Institute of Technology, Experimental Towing Tank Report No. 334, October 1948. Sherman M. Fairchild Publication Fund Paper No. 169, Institute of the Aeronautical Sciences, New York

2. Pierson, John D.. and Leshnover, Samuel. *An Analysis of the Fluid Flow in the Spray Root and Wake Regions of Flat Planing Surfaces.* Stevens Institute of Technology, Experimental Towing Tank Report No. 335, October 1948. Sherman M Fairchild Publication Fund Paper No 166, Institute of the Aeronautical Sciences, New York.

3 Pierson, John D *On the Pressure Distribution for a Wedge Penetrating a Fluid Surface.* Stevens Institute of Technology, Experimental Towing Tank Report No 336. Sherman M Fairchild Publication Fund Paper No 167, Institute of the Aeronautical Sciences, New York.

4. Korvin-Kroukovsky, B.V.; Savitsky, Daniel; and Lehman, William F.
    Wave Contours in the Wake of a 20° Deadrise Planing Surface.
    Stevens Institute of Technology, Experimental Towing Tank Report
    No. 337, June 1948. Sherman M. Fairchild Publication Fund Paper
    No. 168, Institute of the Aeronautical Sciences, New York.

5. Korvin-Kroukovsky, B.V.; Savitsky, Daniel; and Lehman, William F.
    Wave Contours in the Wake of a 10° Deadrise Planing Surface.
    Stevens Institute of Technology, Experimental Towing Tank Report
    No. 344, November 1948. Sherman M. Fairchild Publication Fund Paper
    No. 170, Institute of the Aeronautical Sciences, New York.

6. Korvin-Kroukovsky, B.V.; Savitsky, Daniel; and Lehman, William F.
    *Wake Profile of a Vee Planing Surface, Including Test Data on a
    30° Deadrise Surface.* Stevens Institute of Technology, Experi-
    mental Towing Tank Report No. 339, April 1949. Sherman M. Fairchild
    Publication Fund Paper No. 229, Institute of the Aeronautical
    Sciences, New York.

7. Korvin-Kroukovsky, B.V.; Savitsky, Daniel; and Lehman, William F.
    Wetted Area and Center of Pressure of Planing Surfaces. Stevens
    Institute of Technology, Experimental Towing Tank Report No. 360,
    August 1949. Sherman M. Fairchild Publication Fund Paper No. 244,
    Institute of the Aeronautical Sciences, New York.

8. Wagner, Herbert. *The Phenomena of Impact and Planing on Water.* NACA
    Translation 1366, National Advisory Committee for Aeronautics,
    Washington, D.C. ZAMM, August 1932.

9. Lamb, Horace. *Hydrodynamics.* 6th Ed., Dover Publications, New York,
    1945.

APPENDIX I

SAMPLE CONSTRUCTION OF THE FREE SURFACE SHAPE

This appendix presents the details of the computations and drafting methods employed in the construction of the free surface shape that meets the conditions of continuity, similarity, and irrotationality. To obtain greater clarity, not all of the construction lines are drawn and some of the tables are abbreviated.

FIRST ESTIMATE OF THE SURFACE SHAPE

As noted in the body of the report, the free surface is built up of spray and wave. The first estimate of the wave rise is given by Equation (3). For this particular case, c is taken as 10 inches for $\beta = 40^\circ$ and

$$\eta_0 = \frac{2c \, \tan\beta}{\pi} \left(\frac{x}{c} \arcsin \frac{c}{x} - 1 \right) = 5.34 \left(\frac{x}{10} \arcsin \frac{10}{x} - 1 \right) \quad .$$
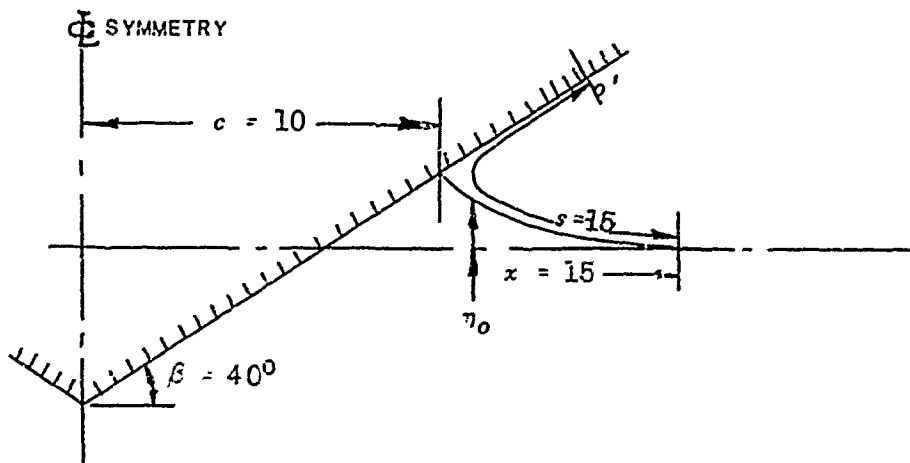
FIGURE I-1

The spray tip, o', is located by measuring along the wave and wedge from $x = 15$ a distance $s = x = 15$. (At the distance $x = 15$, the wave slope is very small so that $s = x$ is a very close approximation.) A spray thickness ratio, $\delta/c = 0.055$, was assumed.

The addition of spray requires that the wave rise be reduced to satisfy continuity of the flow. In order to keep a simple analytic form for the wave at a distance, the value of η_0 is reduced proportionately:

$$\eta_1 = a\eta_0$$

and the spray is blended into the reduced wave to form the spray-root region.
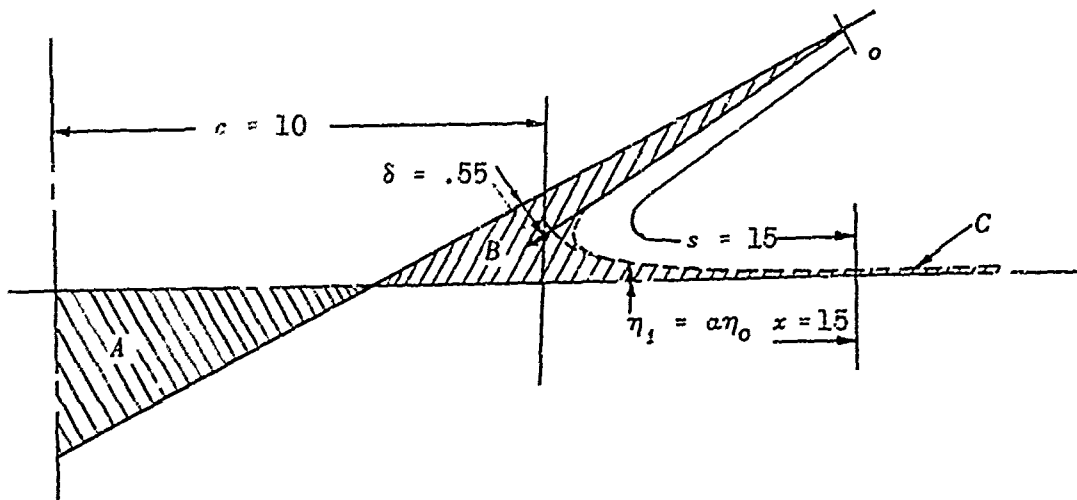
FIGURE I-2

The spray tip is located more exactly by following the curved surface, and area B plus C is made to equal area A by varying the wave rise η_1/η_0 and to a small extent, by the spray-root curve. The area C beyond $x = 15$ on the wave-rise curve may be obtained by the integral of Equation (3):

$$\text{Area } C = \int_{\infty}^{x=15} \eta_1 \, dx = a \int_{\infty}^{x=15} \eta_0 \, dx \qquad \text{(see Equation (4))}.$$

APPLICATION OF SIMILARITY CONDITION

The estimated surface shape, as drawn above, is of the correct length and encloses the proper fluid area. It is then necessary to apply the test of Equation (17), using the assumed shape to determine the velocity components (Figure 3). The actual calculations for this particular case are given in Table I.

If the first approximation to the surface shape is in error, the values of η and ξ resulting from this graphical integration will differ from the assumed values. Then, the process is repeated, using the newly calculated coordinates of the free surface until a close check is obtained in Table I between the starting and final η and ξ.

APPLICATION OF CONDITION FOR IRROTATIONAL FLOW

The superposition of the potential flow due to a doublet upon the flow pattern determined by the free surface shape obtained above must satisfy Equation (31) for irrotational flow. The quantities $t\phi$ and $t(\partial\phi/\partial n)$ for the trial surface shape are obtained by Equations (20) and (15) as shown in Figure I-1 (resolving tU parallel and normal to the surface). The values of ϕ_d and $\partial\phi_d/\partial n$ for the doublet are given by Equations (25) and (28) and are computed in Table II. The values of $t\phi$ and $t(\partial\phi/\partial n)$ are computed in Table III.

From Figure I-1, the left-hand side of Equation (31) (multiplied by t) may be evaluated. For the particular case of $\delta/c = 0.055$ for $\beta = 40^\circ$ ($c = 10$ inches), the value of $t\left.\dfrac{\partial\phi}{\partial s}\right|_d$ at the doublet (with respect to the doublet) is

$$t\left.\frac{\partial\phi}{\partial s}\right|_d = s_d - y_o\cos\beta = -6.18 \qquad .$$

Also, $tV\cos\beta = y_o\cos\beta = 4.09$ and $\mu = 2.86$ radians. Thus,

$$-\left.\frac{\partial\phi}{\partial s}\right|_d + 2V\mu\cos\beta = \frac{-(-6.18)}{t} + \frac{2\,(4.09)(2.86)}{t}$$

$$= \frac{+42.8}{t} \qquad .$$

The right-hand side of Equation (31) is evaluated by computing the values of $[t\phi(\partial\phi_d/\partial n) - \phi_d\,t(\partial\phi/\partial n)]$ and integrating along the surface. This is done in Table III, making use of the values of ϕ_d and $\partial\phi_d/\partial n$ from Table II. In this particular case, an approximately correct spray thickness was chosen so that value of the integral

$$\int\left(\phi\,\frac{\partial\phi_d}{\partial n} - \phi_d\,\frac{\partial\phi}{\partial n}\right)ds = \frac{42.1}{t}$$

is very close to the left-hand side value, $42.8/t$, given above.

In general, however, several spray thicknesses would be assumed and the complete process carried out to this stage. Then plots of the left- and right-hand sides of Equation (31) vs. δ/c would determine by their crossing the correct value of the spray thickness ratio.

TABLE I

TABULAR INTEGRATION FOR SURFACE SHAPE (EQUATION (17))

($\beta = 40°$, $c = 10$ inches, $\delta = 0.55$ inches)

s	η START	tv	$\dfrac{tv}{s^2}$	$\dfrac{tv}{s^2}\Delta s$	$\Sigma\dfrac{tv}{s^2}\Delta s$	η NEW	$\xi - \xi_0$ START	tu	$\dfrac{tu}{s^2}$	$\dfrac{tu}{s^2}\Delta s$	$\Sigma\dfrac{tu}{s^2}\Delta s$	$\xi - \xi_0$ NEW
15.0	0 37	1.43	0.0064		0.0247	0.37						
				0.018								
13.0	0.56	2.13	0.0126		0.0427	0.56	0	0.09	0.0005		0	0
				0.018						0.001		
12.0	0 72	3.21	0.0224		0.0607	0.73	0.01	0.26	0.0018		0.001	0.012
				0.014						0.0015		
11.5	0.86	4.12	0.0312		0.0747	0.86	0.03	0.50	0.0038		0.0025	0.029
				0.0185						0.0030		
11.0	1 02	5.45	0.0450		0.0932	1.025	0.06	1.00	0 0083		0.0055	0 060
				0.8212						0.8644		
10.6	1 21	7.01	0.0624		0.1144	1.21	0.11	1.88	0.0167		0.0099	0.105
				0.0306						0.0116		
10.2	1.48	9.87	0.0949		0.1450	1.48	0.22	4.64	0.0446		0.0215	0.219
				0.0432						0.0276		
9.8	1.85	11.61	0.1210		0.1882	1.85	0.48	9.28	0.0967		0.0491	0.481
				0.0496						0.0508		
9 4	2 24	11.07	0.1252		0.2378	2.24	0.94	13.604	0.1540		0.0999	0.939
				0.0502						0.0692		
9.0	2 59	10.16	0.1255		0.2880	2.59	1.52	15.41	0.1903		0.1691	1.521
				0.064						0.1045		
8.5	2.99	9 42	0.1303		0.3520	2.99	2.33	16.40	0.2272		0.2736	2.325
				0.0683						0.121		
8.0	3.36	9.16	0.1431		0.4203	3.36	3.16	16.68	0.2605		0.3946	3.165
				0.161						0.3025		
7.0	4 07	8.87	0.1810		0.5813	4.07	4.88	16.98	0.346		0.6971	4.88

TABLE II

COMPUTATION OF ϕ_d AND $\partial\phi_d/\partial n$

($\beta = 40°$, $c = 10$ inches, $\delta = 0.55$ inches)

s	R_d	R_{id}	α_d	α_{id}	θ_d	θ_{id}	ϕ_d	$\dfrac{\partial\phi_d}{\partial n}$
3.0	6.90	6.98	169.0	166.0	8.0	17.5	0.063	0.002
5.0	4.93	5.10	165.5	159.0	11.5	24.5	0.121	0.010
7.0	2.99	3.39	158.0	145.0	18.5	38.5	0.294	0.060
8.0	2.06	2.69	149.5	131.0	24.5	54.5	0.527	0.167
8.5	1.60	2.45	143.0	121.5	28.5	67.5	0.724	0.260
9.0	1.16	2.34	132.5	109.5	30.5	88.0	1.039	0.324
9.4	0.82	2.40	121.0	100.0	29.5	109.5	1.455	0.210
9.67	0.58	2.53	111.0	95.0	23.5	130.5	2.004	0.257
9.87	0.39	2.68	102.5	92.0	16.0	150.0	2.876	0.476
10.07	0.20	2.86	96.5	90.0	7.0	165.5	5.318	0.249
10.27	0	3.06	90.0	90.0	0	180.0	0.327±∞	0
10.47	0.20	3.26	96.5	90.5	5.0	10.5	-4.661	-0.671
10.67	0.39	3.45	99.5	91.0	8.5	16.5	-2.239	-0.137
10.87	0.59	3.65	102.5	92.0	10.0	20.0	-1.381	-0.148
11.0	0.71	3.76	105.5	93.0	11.0	23.0	-1.091	-0.180
11.5	1.21	4.21	112.5	96.5	11.0	27.5	-0.528	-0.156
12.0	1.70	4.65	116.0	99.5	12.0	28.5	-0.317	-0.099
13.0	2.69	5.53	121.0	104.5	11.5	28.0	-0.144	-0.054

TABLE III

EVALUATION OF EQUATION (31)

($\beta = 40°$, $c = 10$ inches, $\delta = 0.55$ inches)

s	v	$t\omega$	$-t\dfrac{\partial\phi}{\partial n}$	ϕ_d	$\dfrac{\partial\phi_d}{\partial n}$	$t\phi\dfrac{\partial\phi_d}{\partial n}$	$-\phi_d\,t\dfrac{\partial\phi}{\partial n}$
2.0	16 28	128.7	5.14	0.063	0 002	0.256	0.324
5.0	14.38	91.24	5.14	0.121	0.010	0.912	0.622
7.0	12 53	54.24	5.14	0.294	0 069	3 255	1.513
8.0	11 63	35.89	5.72	0.527	0 167	5.994	3 014
8 5	11.20	26.80	6 18	0.724	0 260	6 968	4.474
9.0	10.82	18.13	7.40	1.039	0.324	5.874	7 689
9 4	10 56	11.90	8.90	1.455	0.210	2.499	12 95
9 67	10.45	8 03	10.08	2.004	0.257	2.064	20.20
9.87	10.42	5.54	10.98	2.876	0 476	2.685	31.58
10 07	10 45	4.03	10.00	5 318	0 249	10.69	53 18
10 27	10.55	2.58	8 96	$0.327\pm\infty$	0	0	2 93 0$\pm\infty$
10 47	10.68	2.36	7.57	-4.661	-0 671	-1.584	-35 28
10 67	10.82	1.81	6.77	-2.239	-0.137	-0.248	-15.16
10 87	10.98	1.21	6.08	-1.381	-0.148	-0.179	- 8.396
11 0	11.08	1.19	5.40	-1.091	-0.180	-0 214	- 5 891
11 5	11.55	0.83	4.10	-0.528	-0 156	-0.129	- 2 165
12 0	12 05	0.56	3.20	-0.317	-0.099	-0 055	- 1.014
13.0	13 01	0.30	2 13	-0.144	-0 054	-0 016	- 0 307

FIGURE I

MOTION OF
WEDGE

NO SPRAY

SURFACE WAVE

$$y_0 = \frac{2}{\pi} c \tan \beta$$

MOTION OF
WEDGE

ALL SPRAY

UNDISTURBED FREE SURFACE

$$y_0 = \frac{2}{\pi} c \tan \beta$$
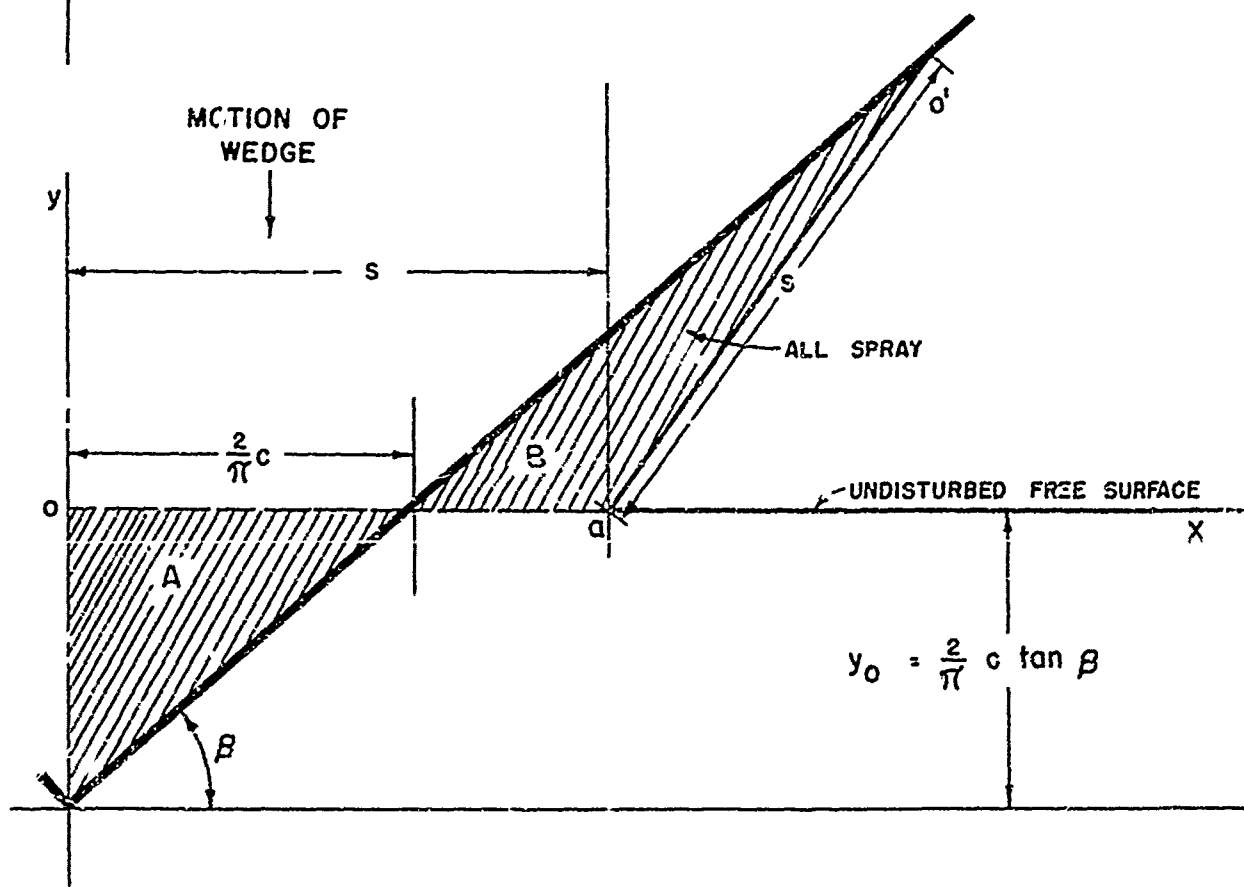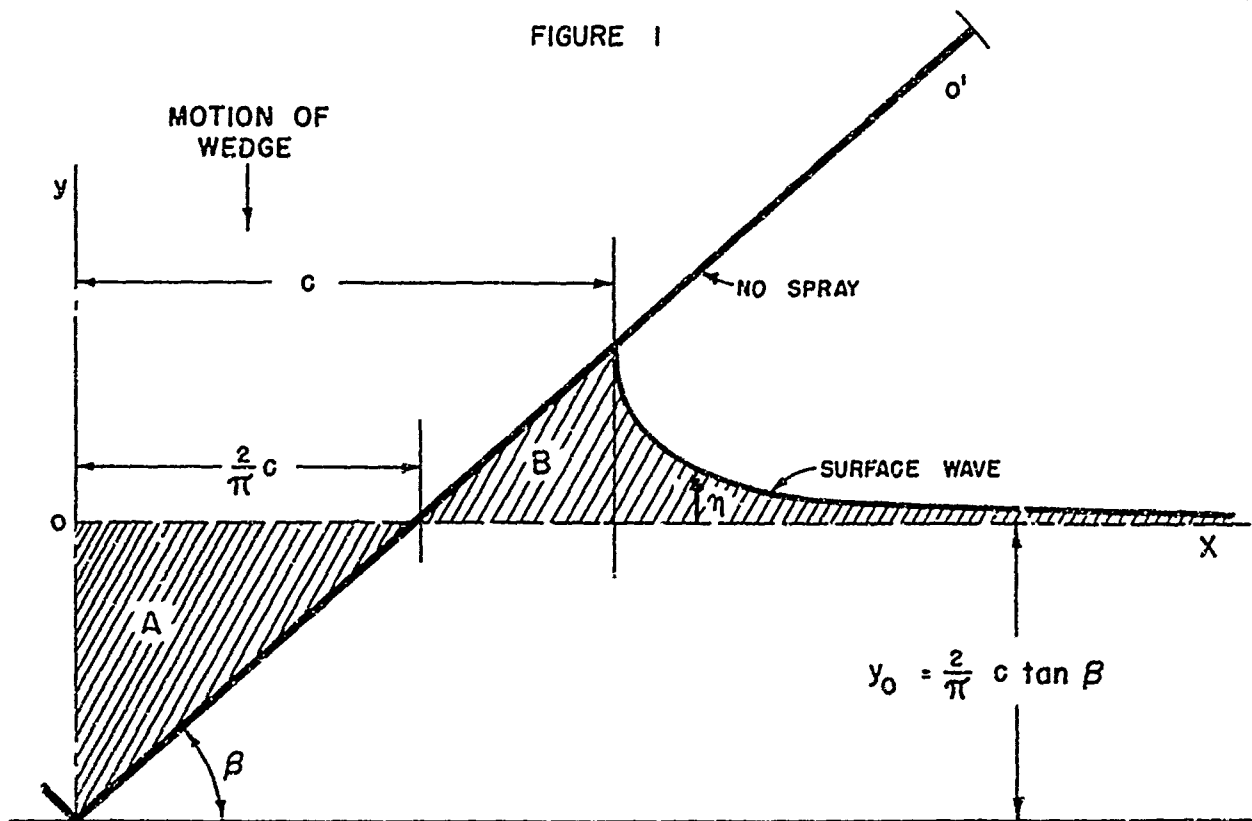
FREE SURFACE SHAPE—EXTREME CASES

FIGURE 2
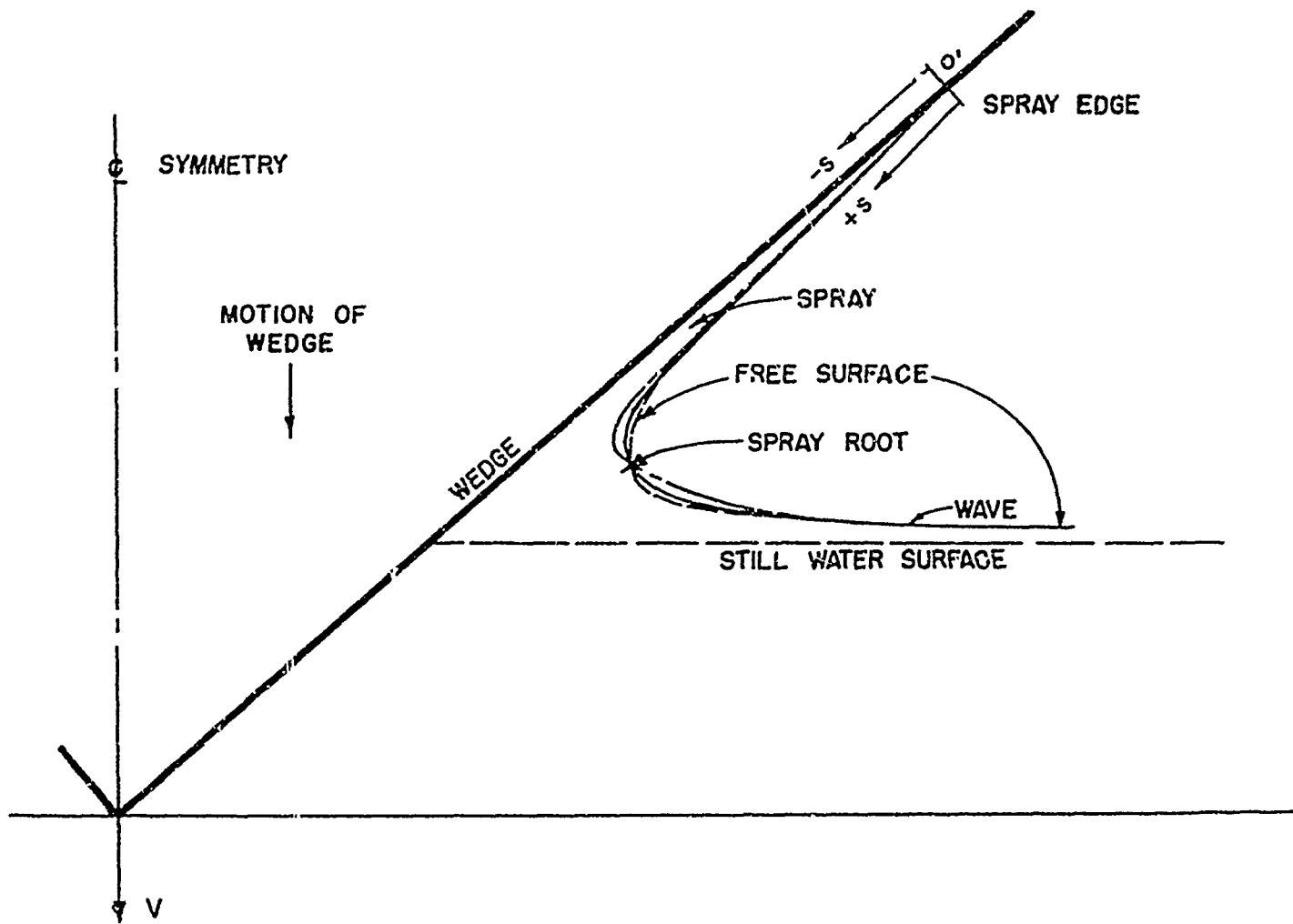
GENERAL SHAPE OF THE FREE SURFACE OF A FLUID
DUE TO PENETRATION BY A WEDGE

FIGURE 3
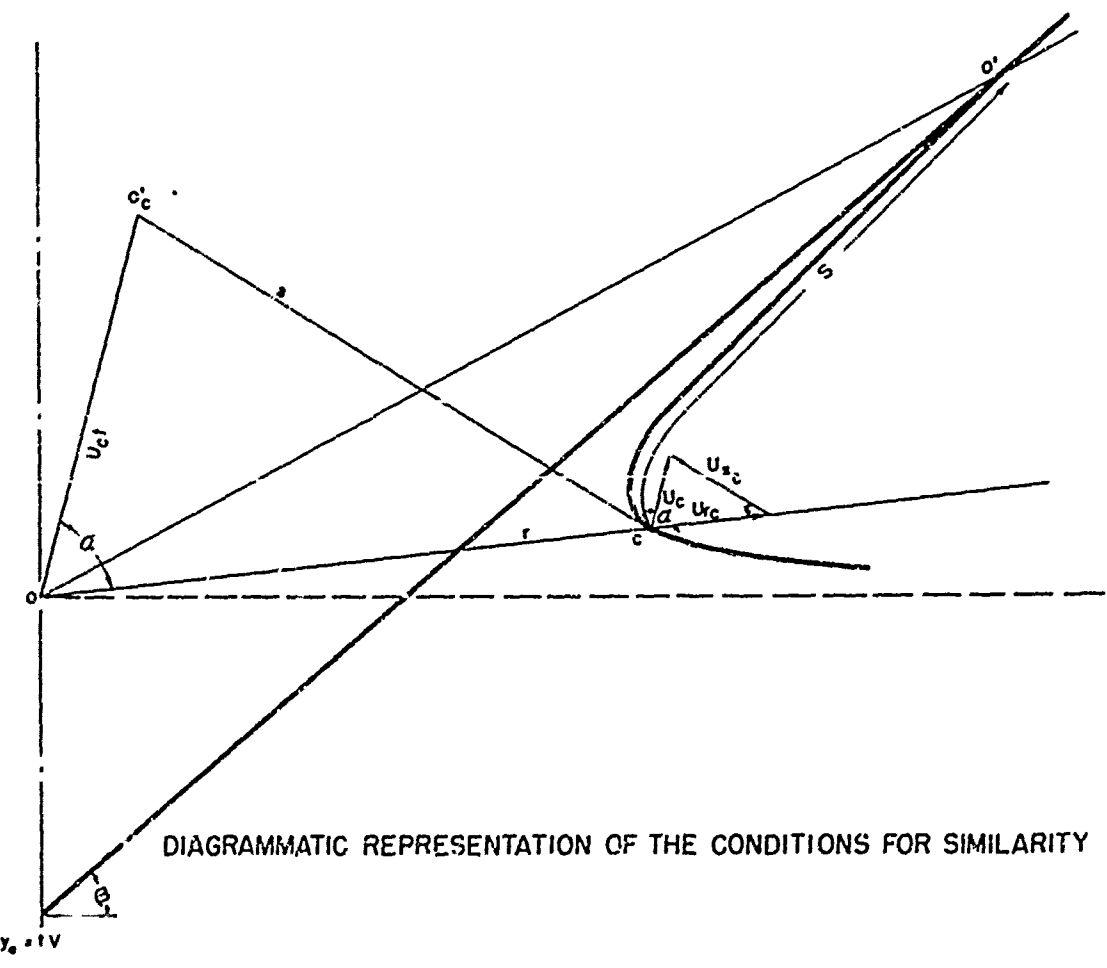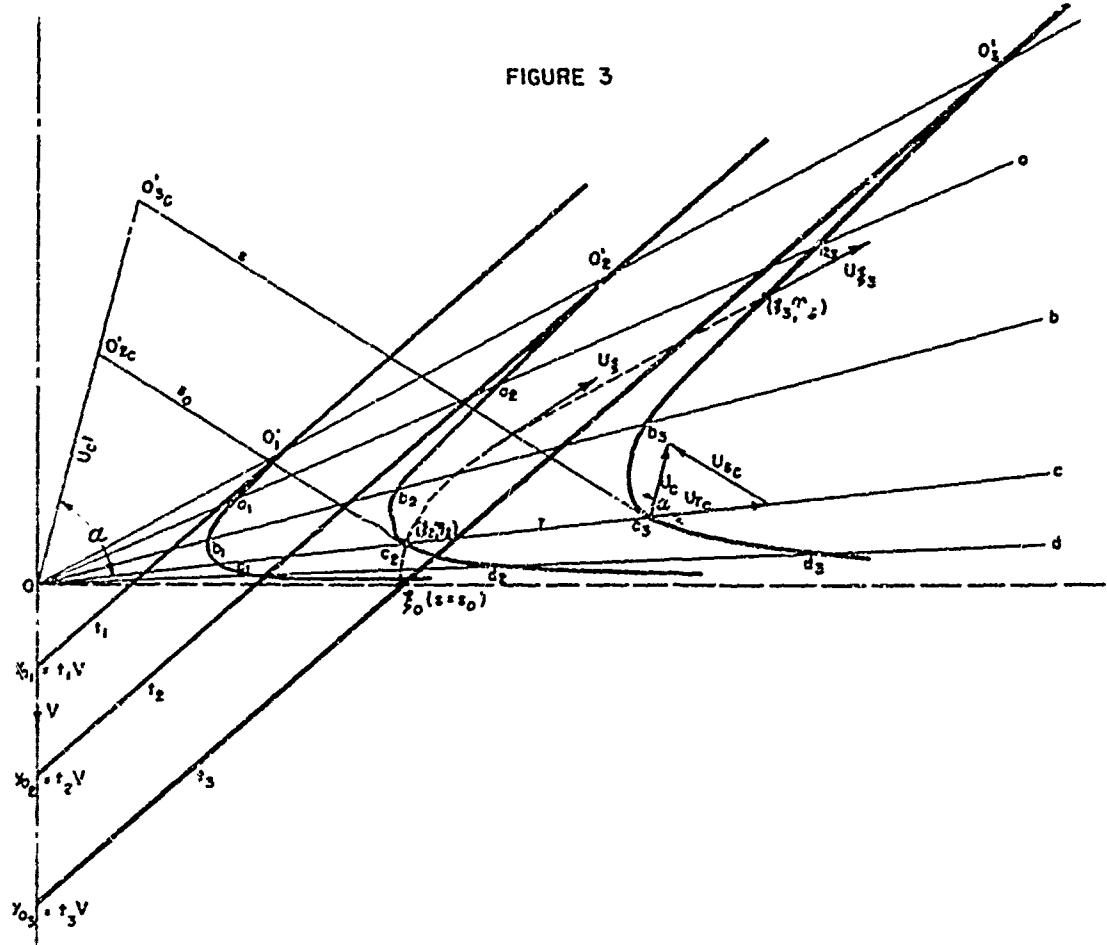
DIAGRAMMATIC REPRESENTATION OF THE CONDITIONS FOR SIMILARITY

FIGURE 4
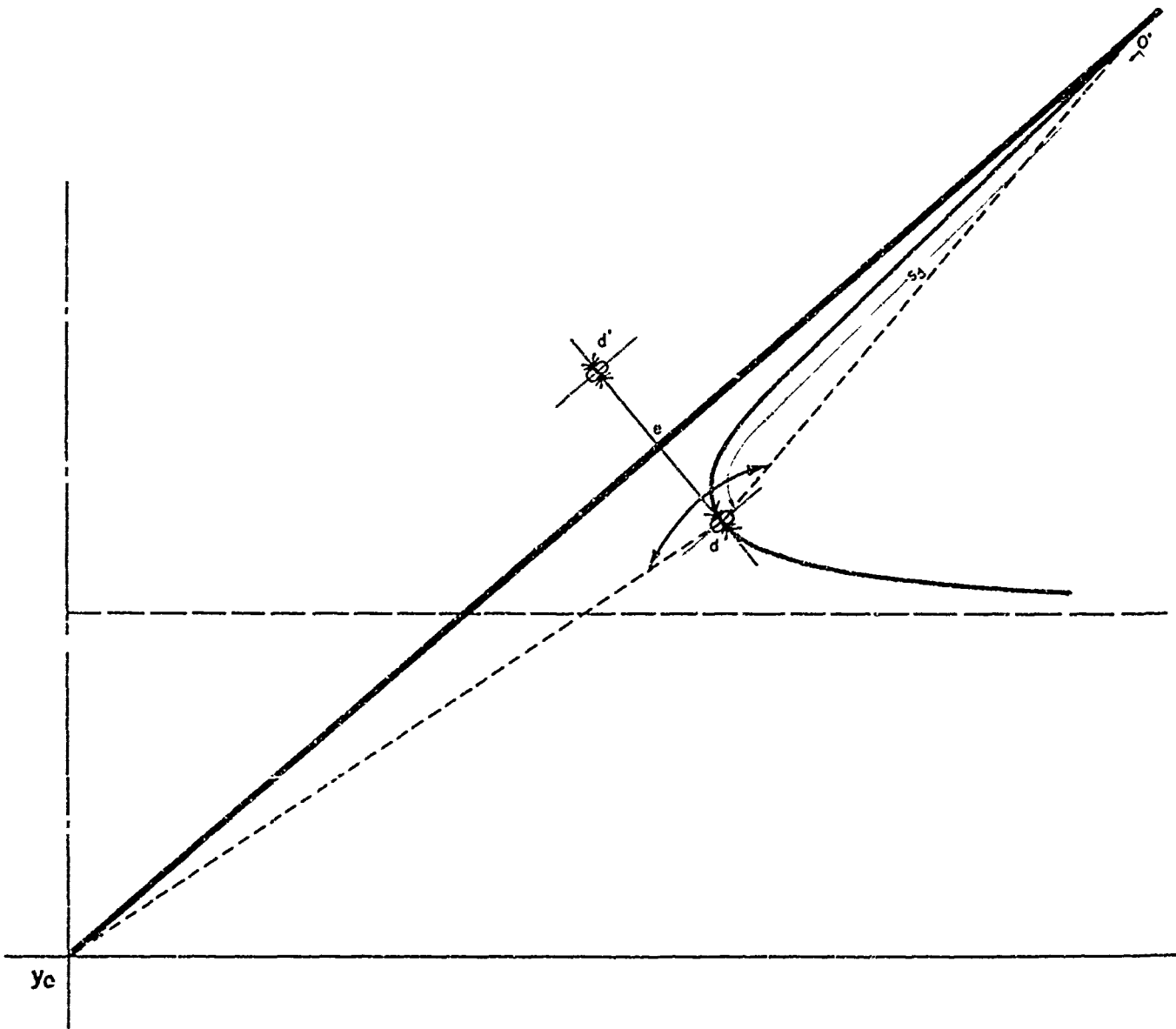
LOCATION OF DOUBLETS FOR IRROTATIONALITY CHECK

FIGURE 5
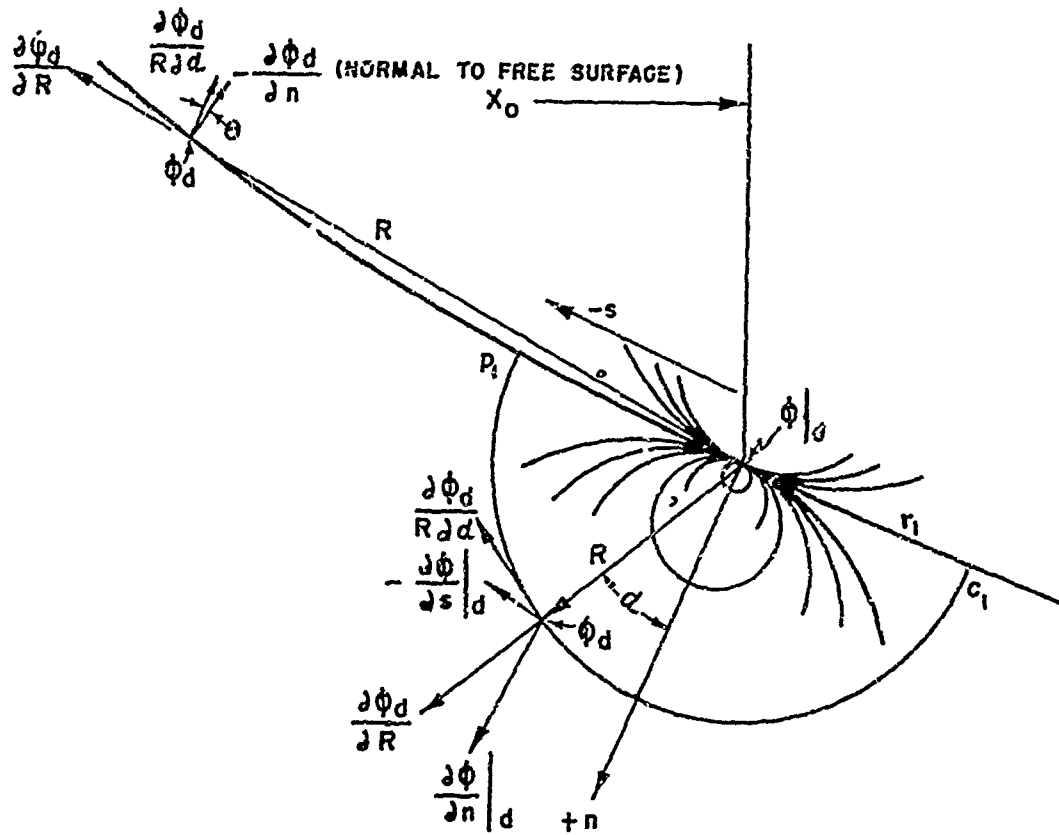
FLOW FIELD IN THE VICINITY OF THE DOUBLET
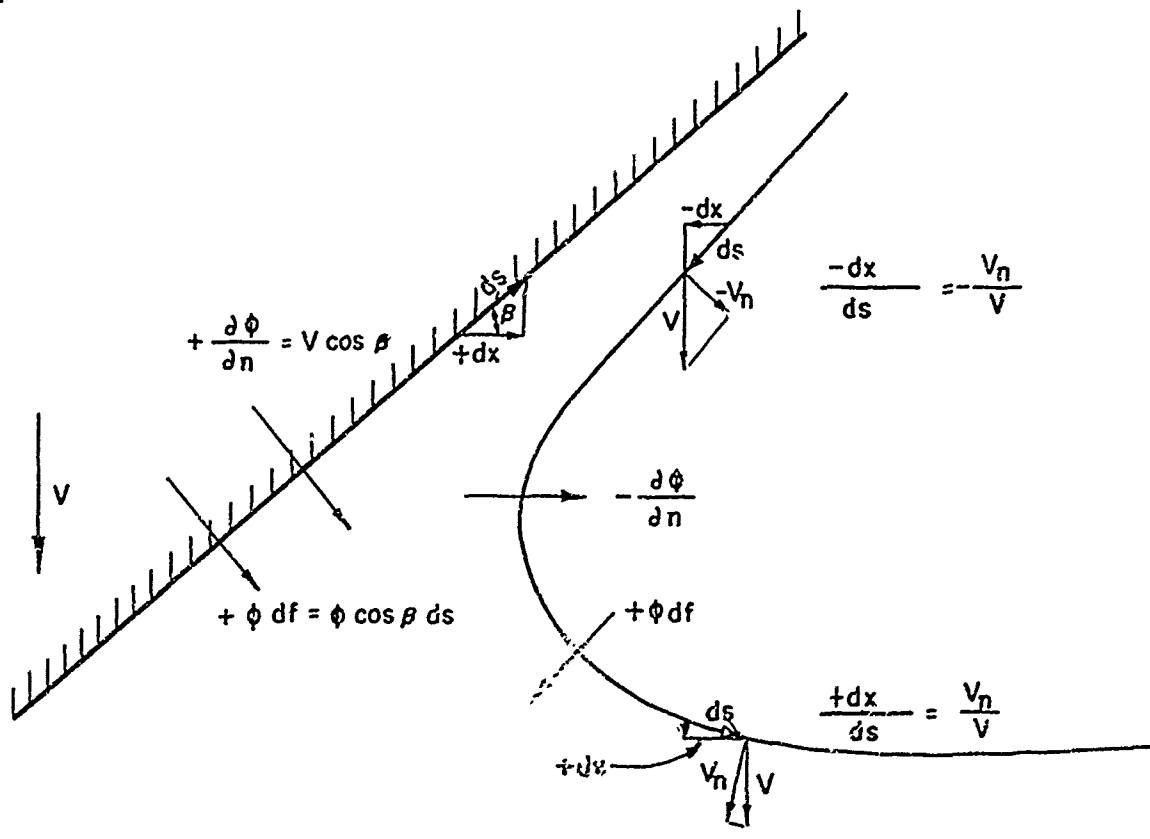
FIGURE 6

SIGN CONVENTIONS FOR SURFACE ELEMENTS AND VELOCITIES
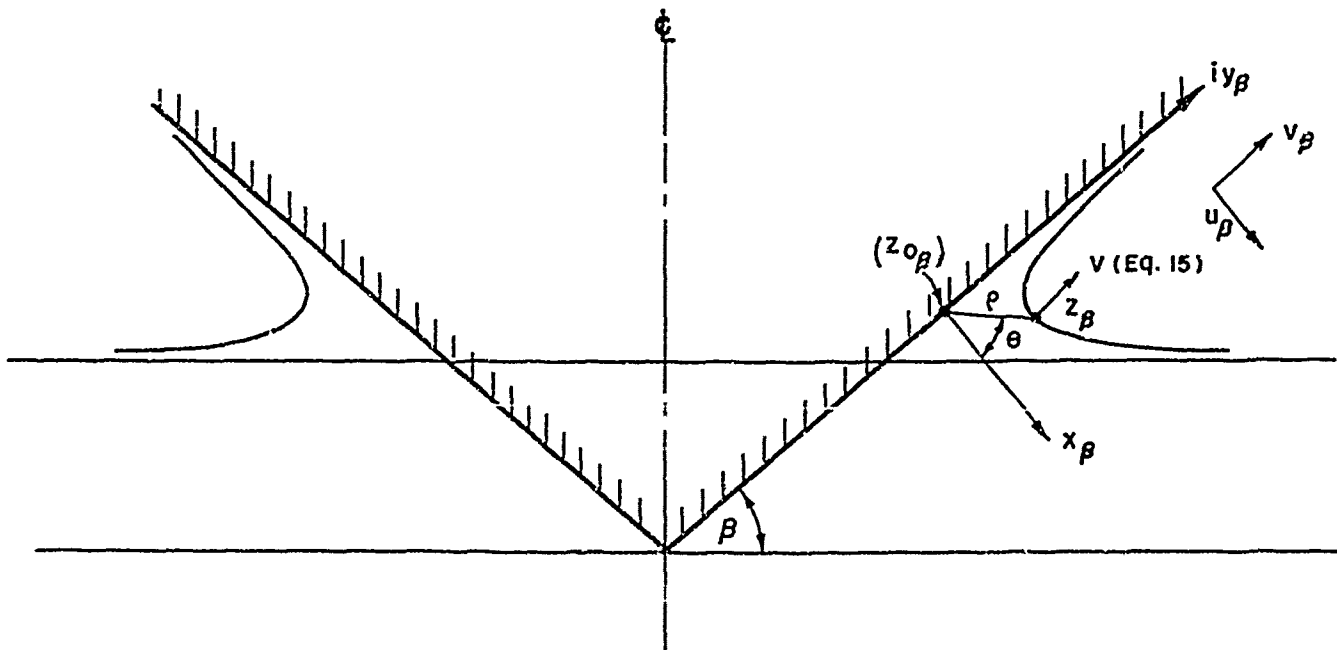
FIGURE 7

POLAR COORDINATE SYSTEM FOR SOLUTION
OF CAUCHY INTEGRAL EQUATION

FIGURE 8

COMPARISON OF FIXED AND RELATIVE POSITION POINTS
IN THE FLUID
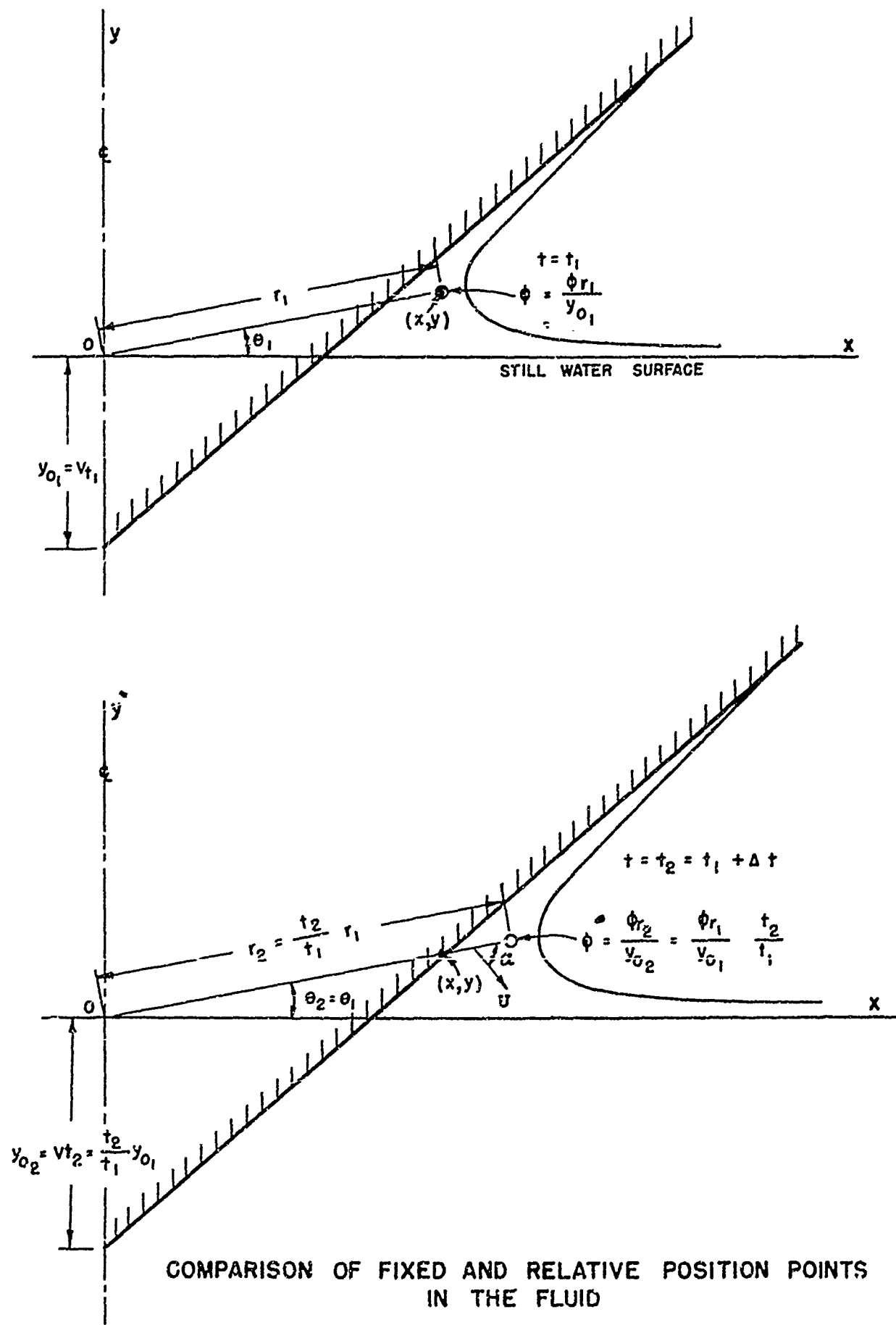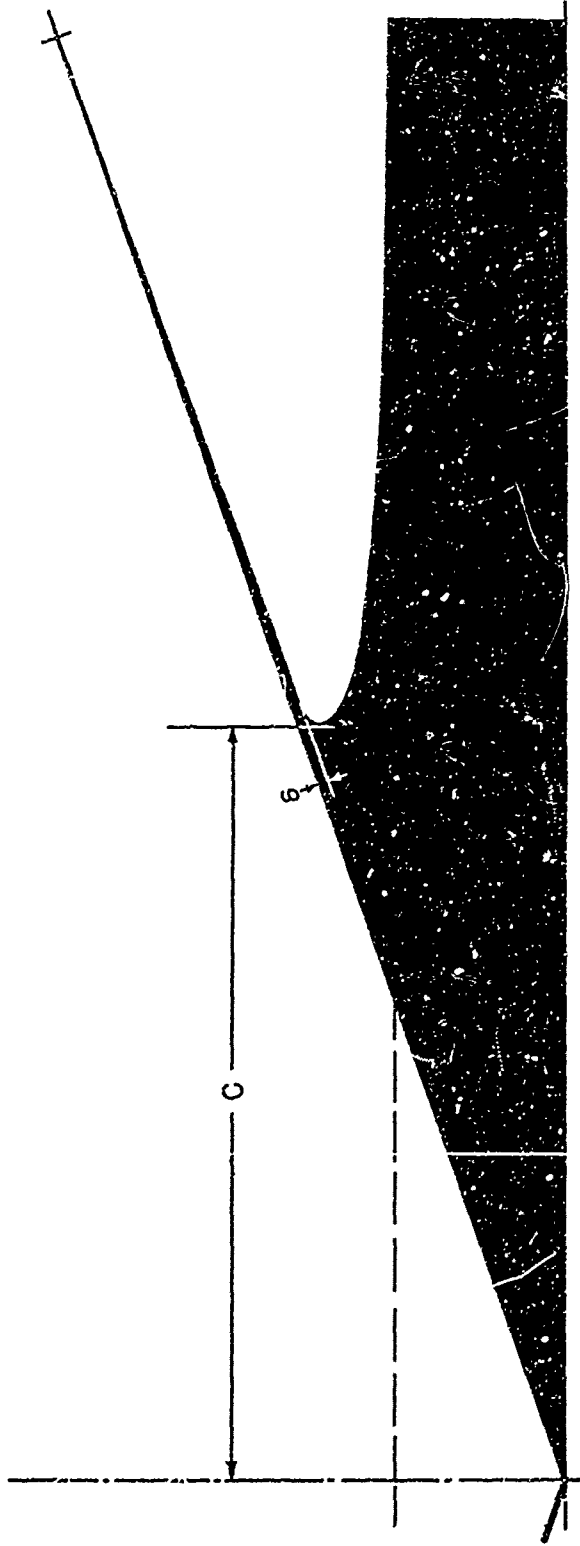
FIGURE 9a

SURFACE SHAPE FOR 20° DEADRISE

FIGURE 9b
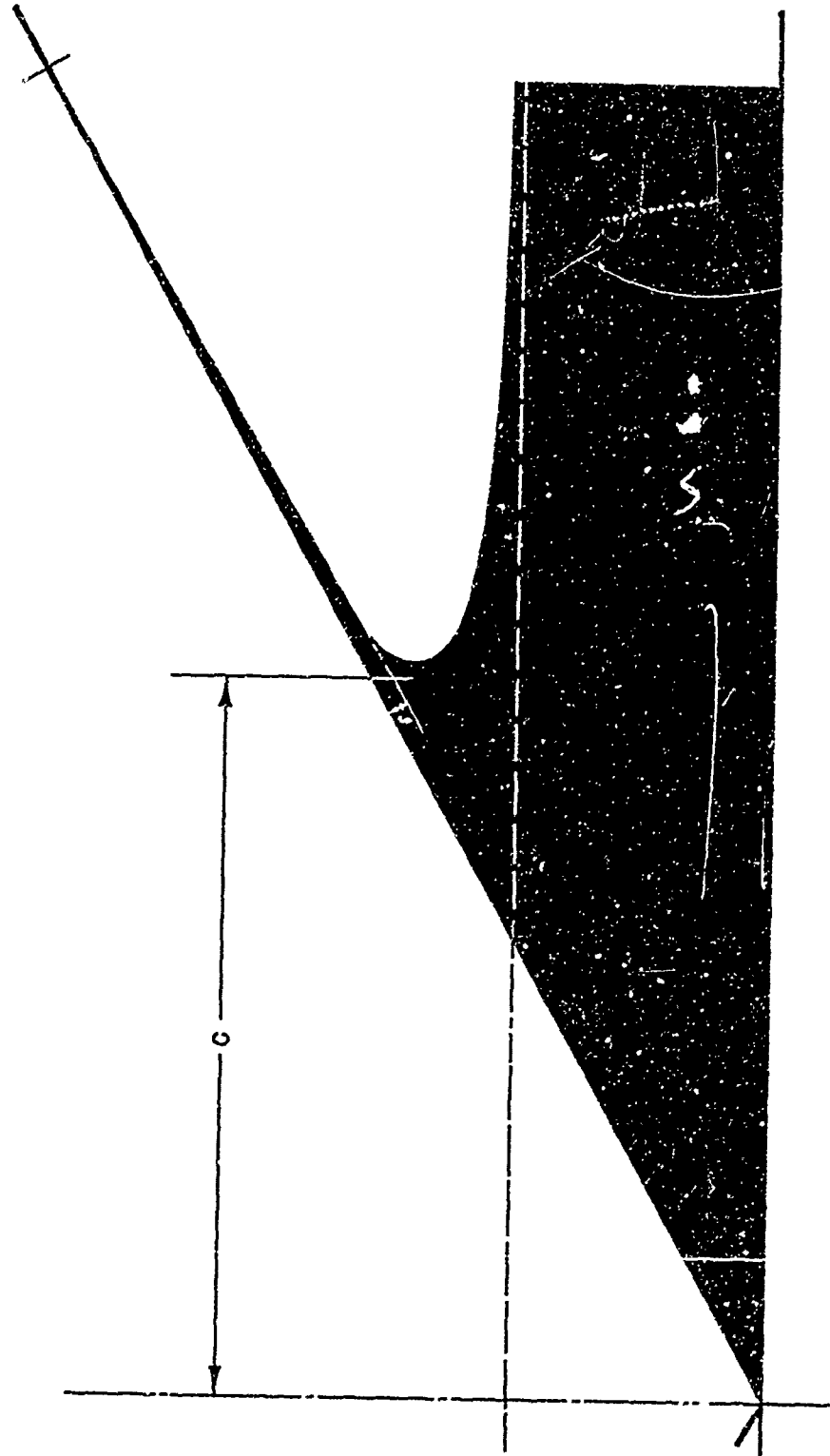
SURFACE SHAPE FOR 30° DEADRISE

FIGURE 9c
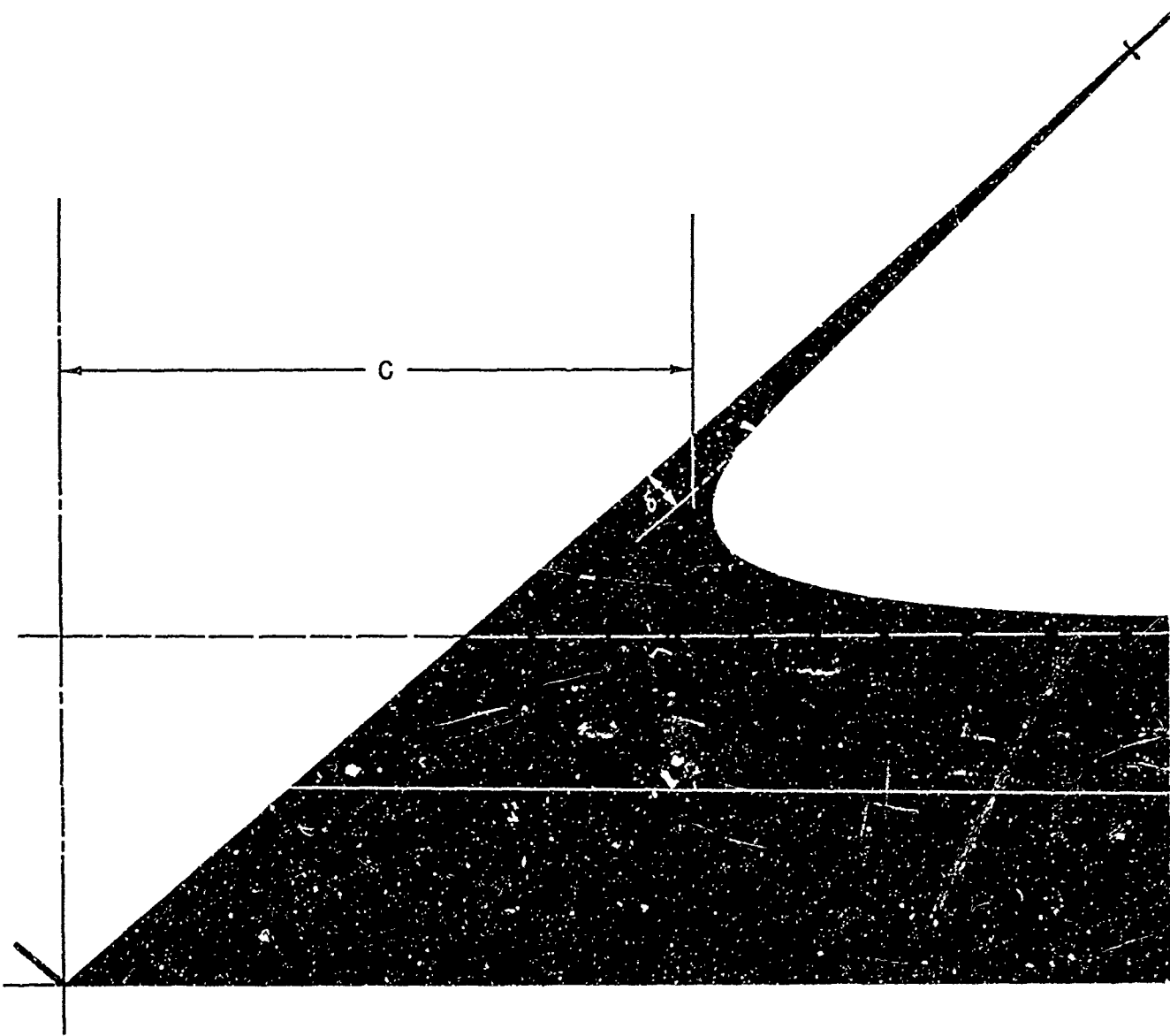
SURFACE SHAPE FOR 40° DEADRISE

FIGURE 9d
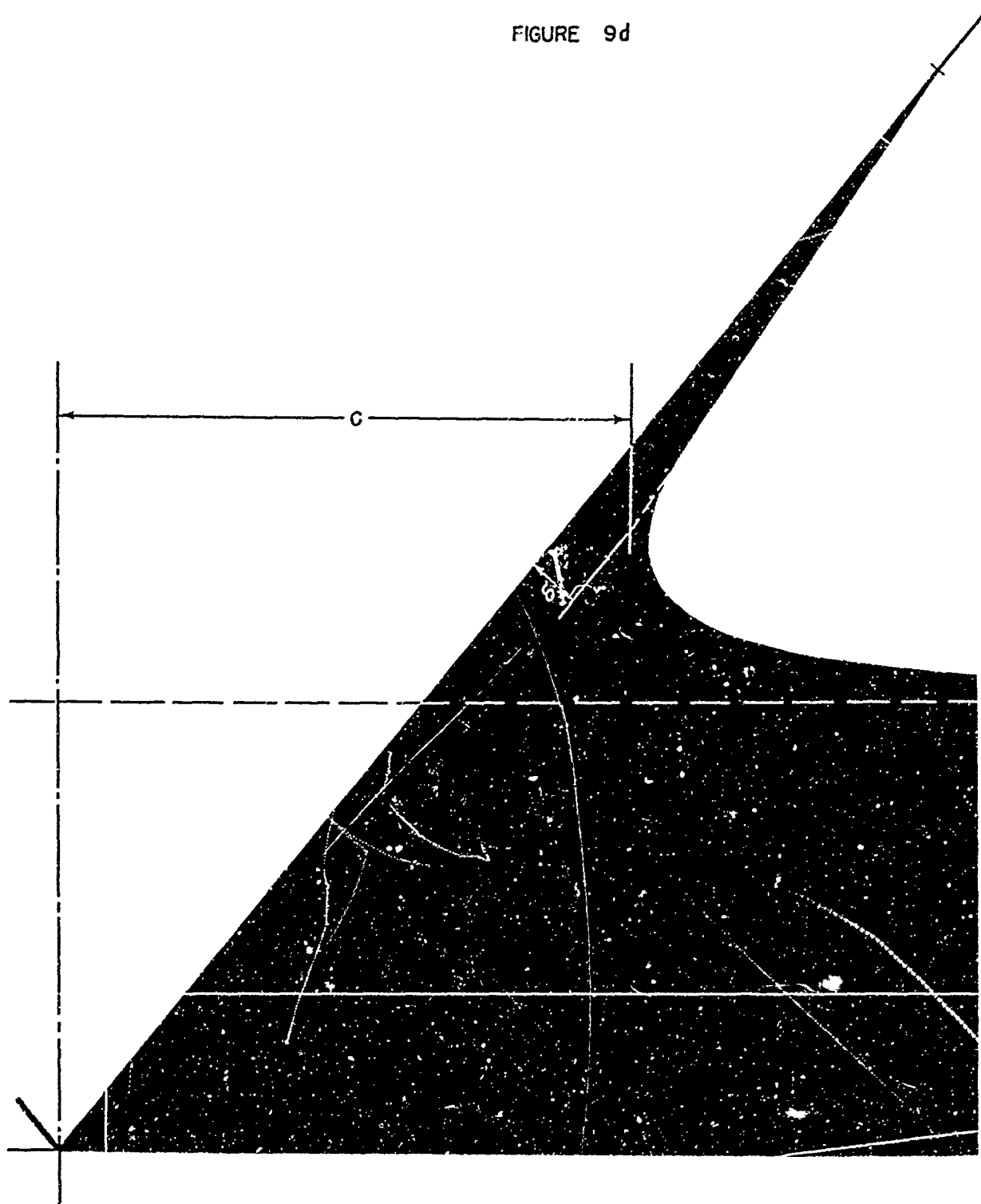
SURFACE SHAPE FOR 50° DEADRISE

FIGURE 10

VARIATION OF SPRAY THICKNESS WITH DEADRISE ANGLE
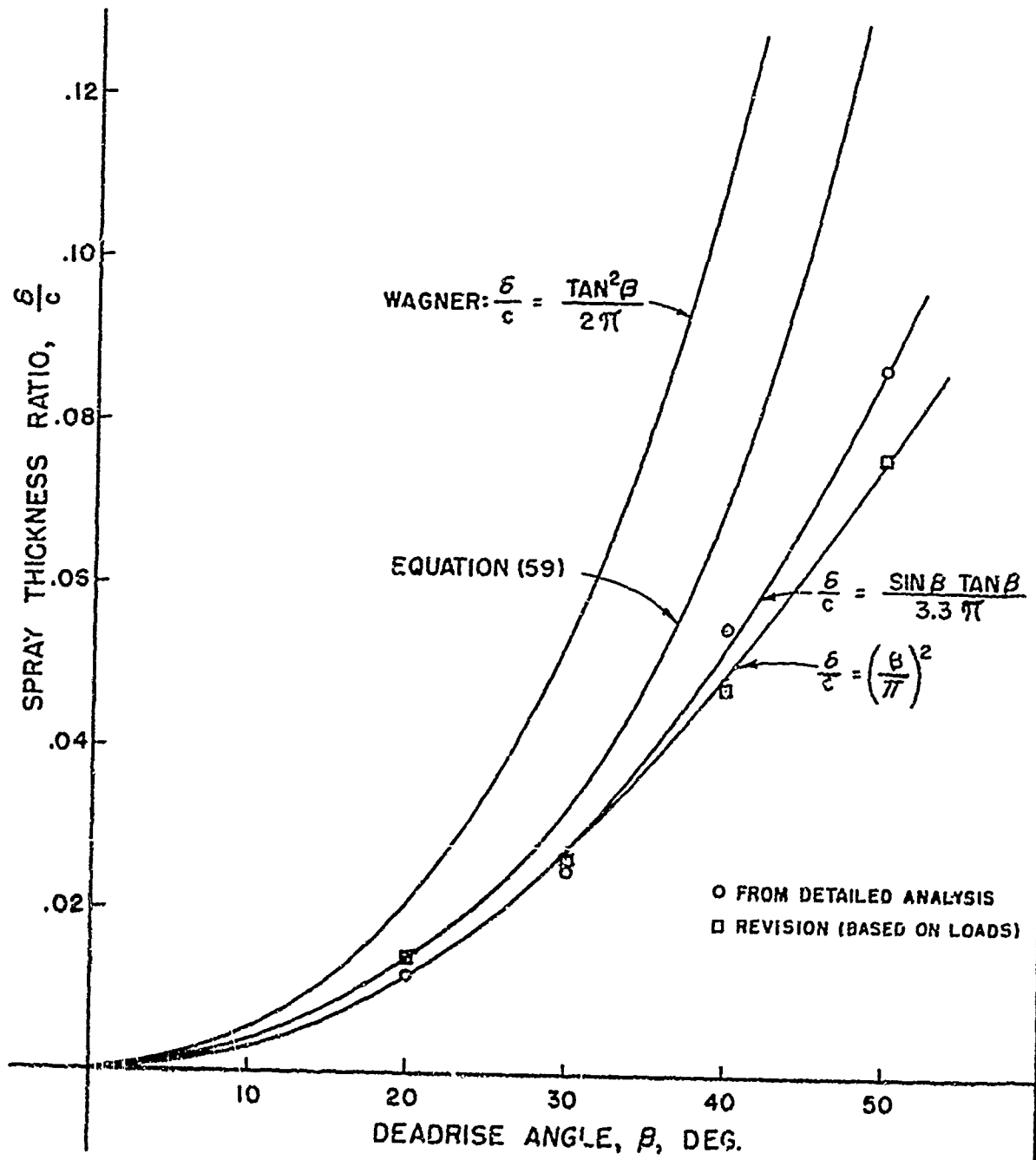
FIGURE II
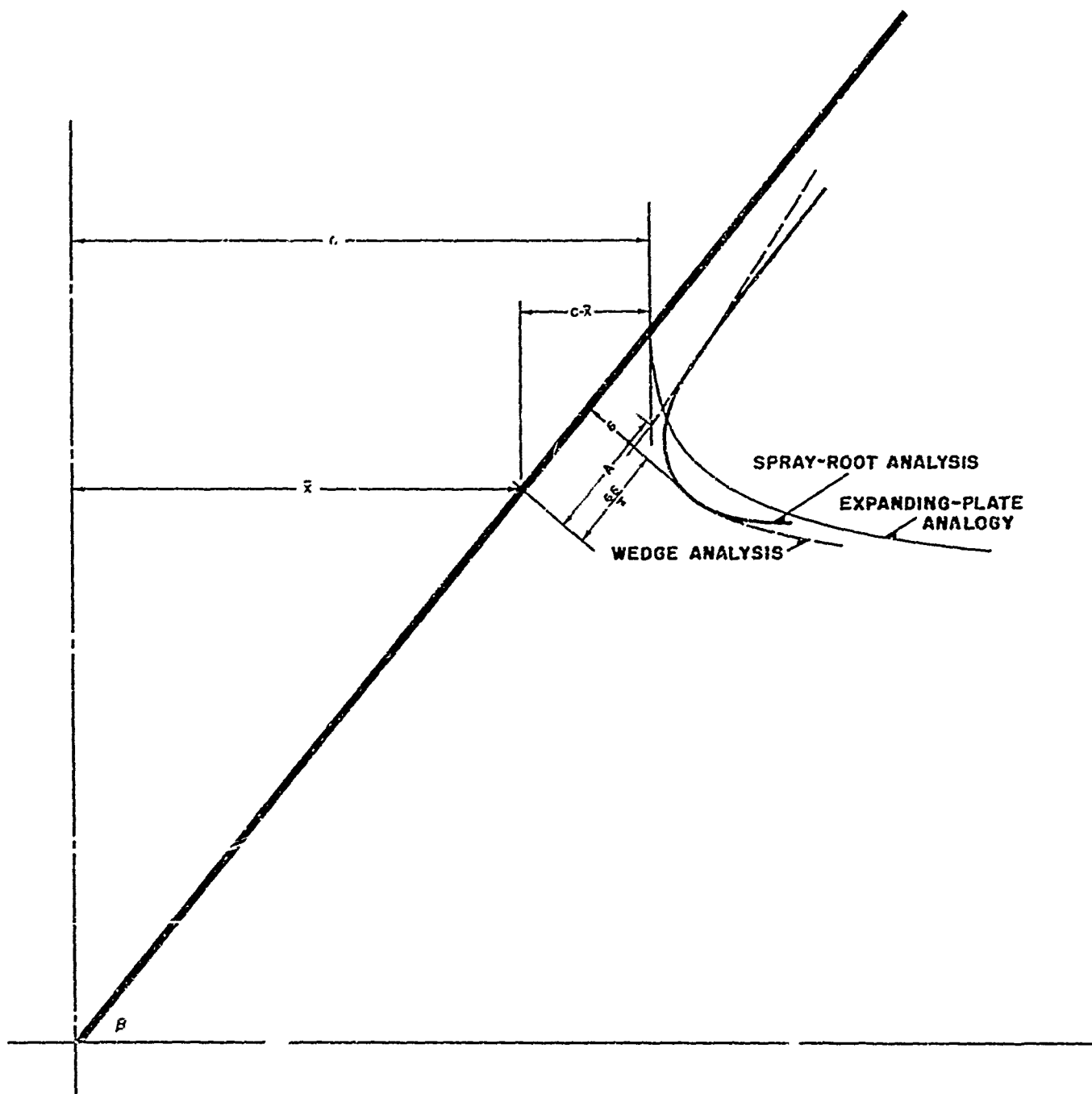
SUPERPOSITION OF SEVERAL SPRAY-ROOT SOLUTIONS
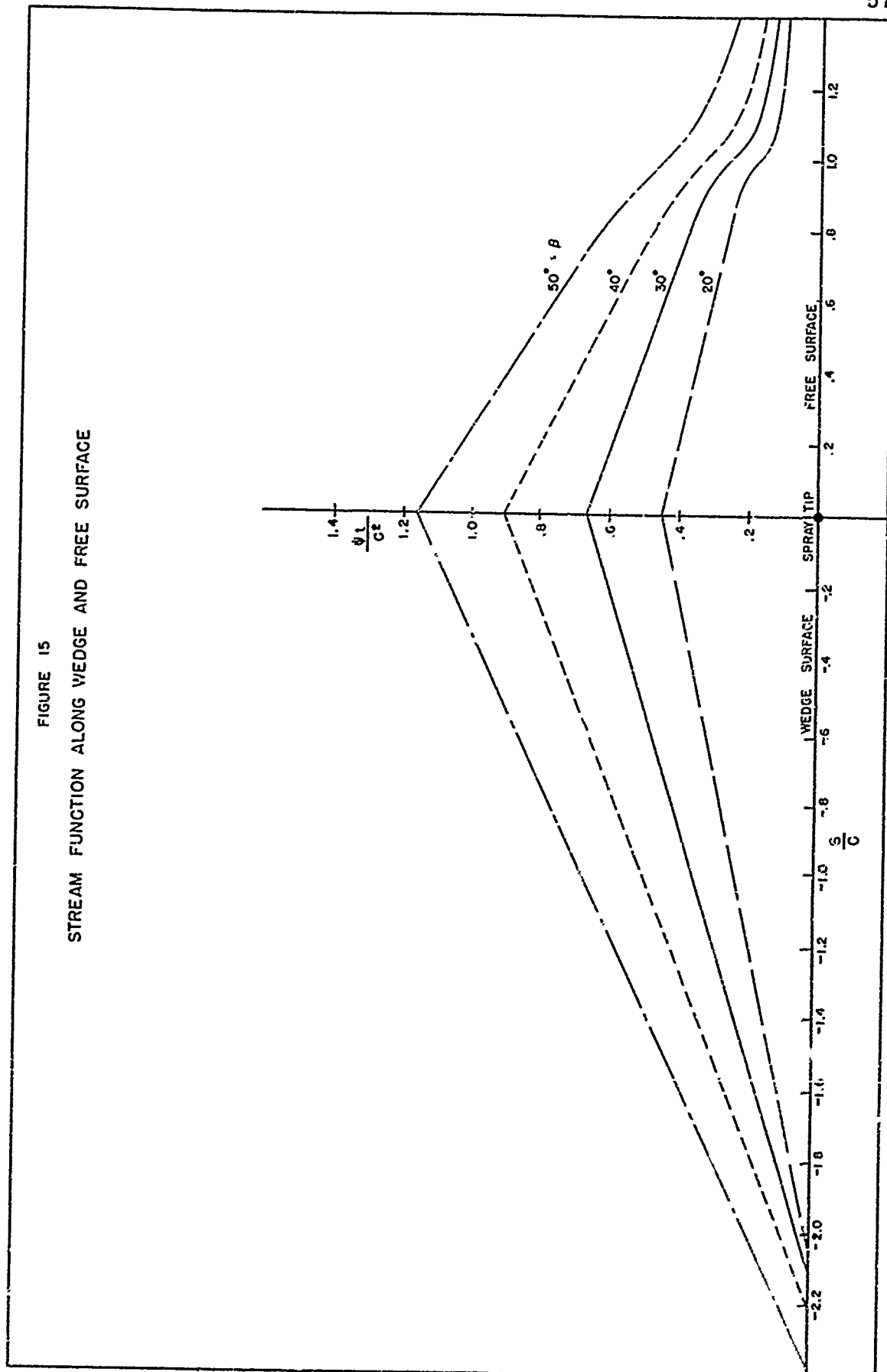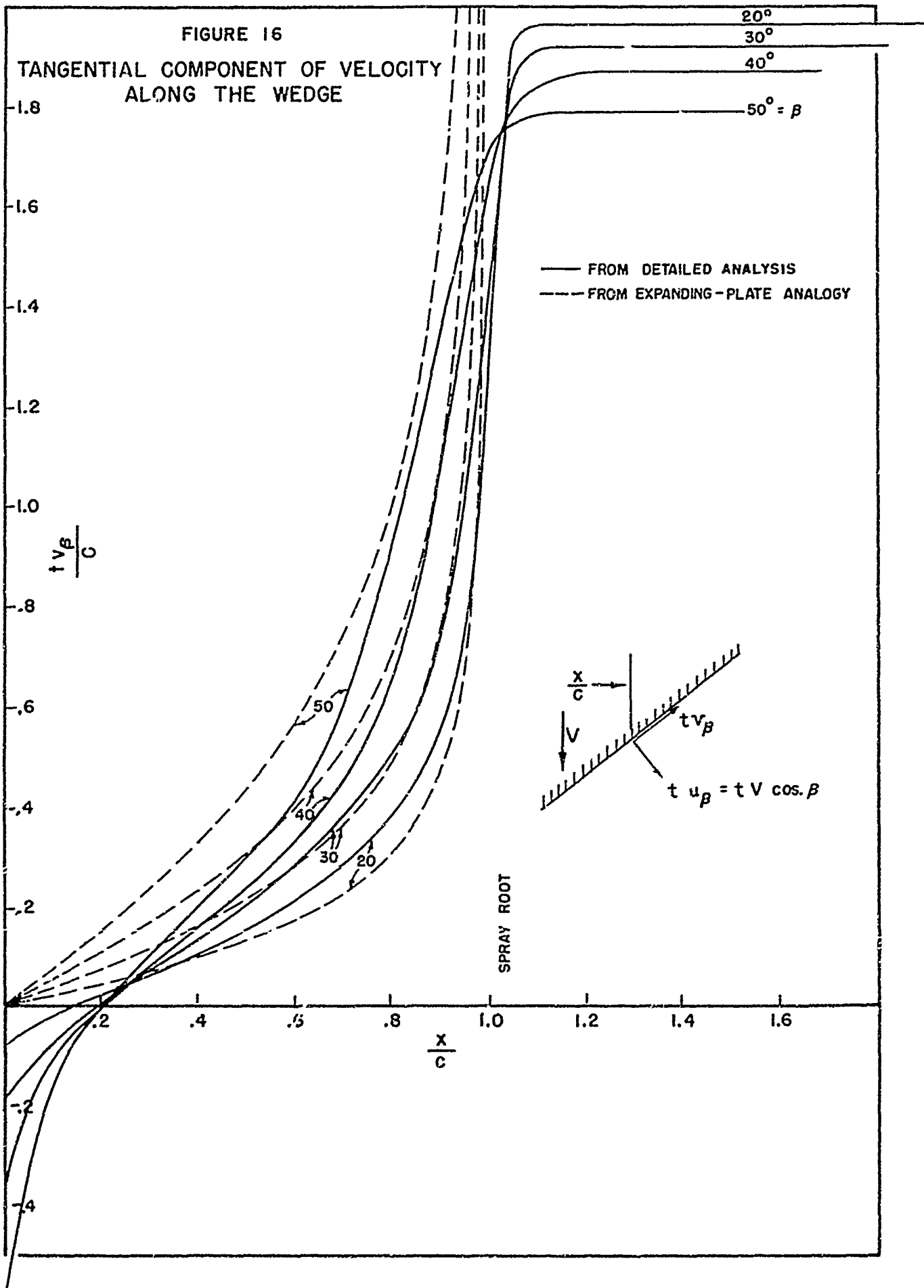
FIGURE 12

VELOCITY DISTRIBUTION ON WEDGE AND FREE SURFACE

FIGURE 13

VELOCITY DIRECTION AT WEDGE AND FREE SURFACE

FIGURE 14

VELOCITY POTENTIAL ON WEDGE AND FREE SURFACE
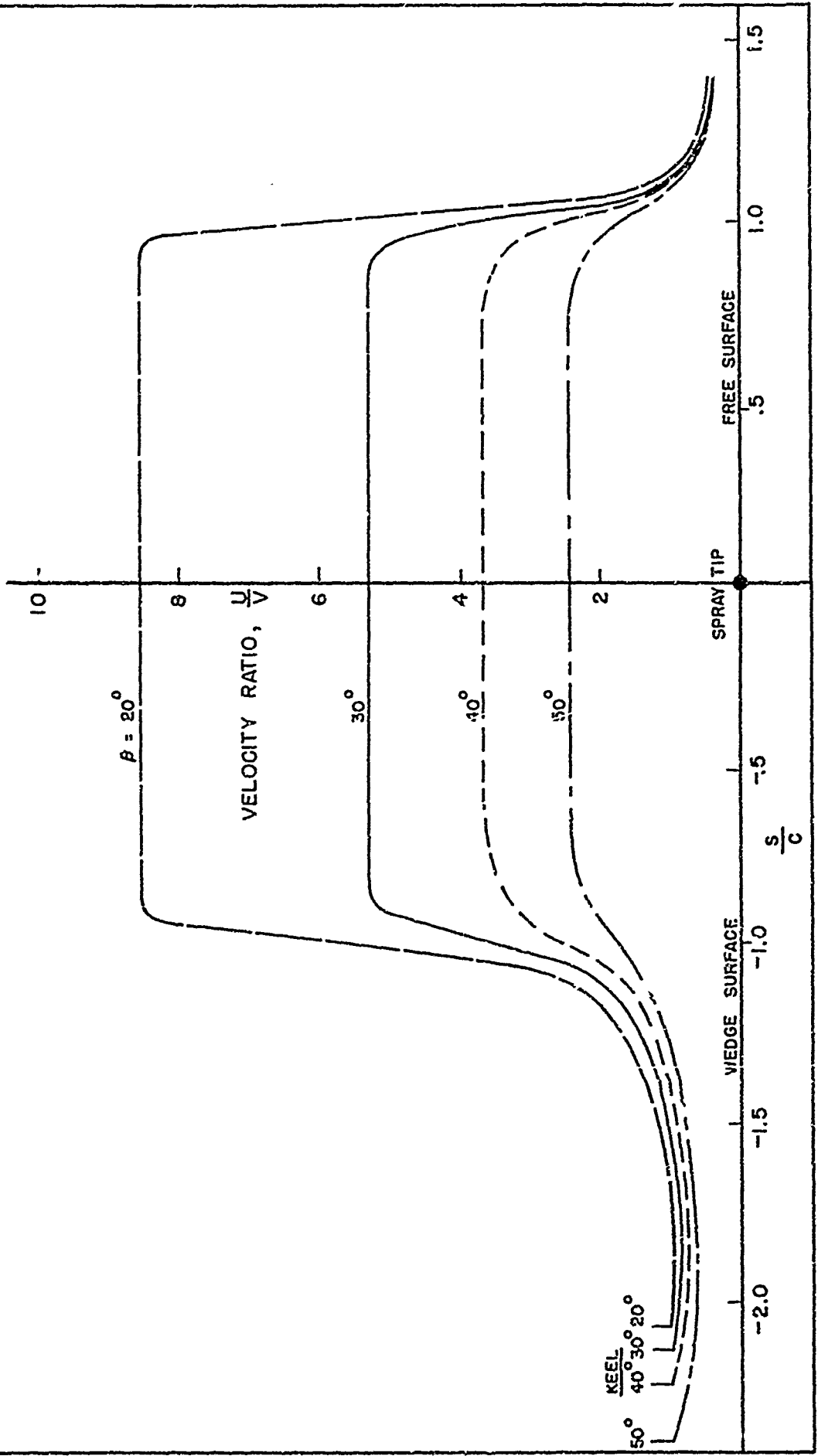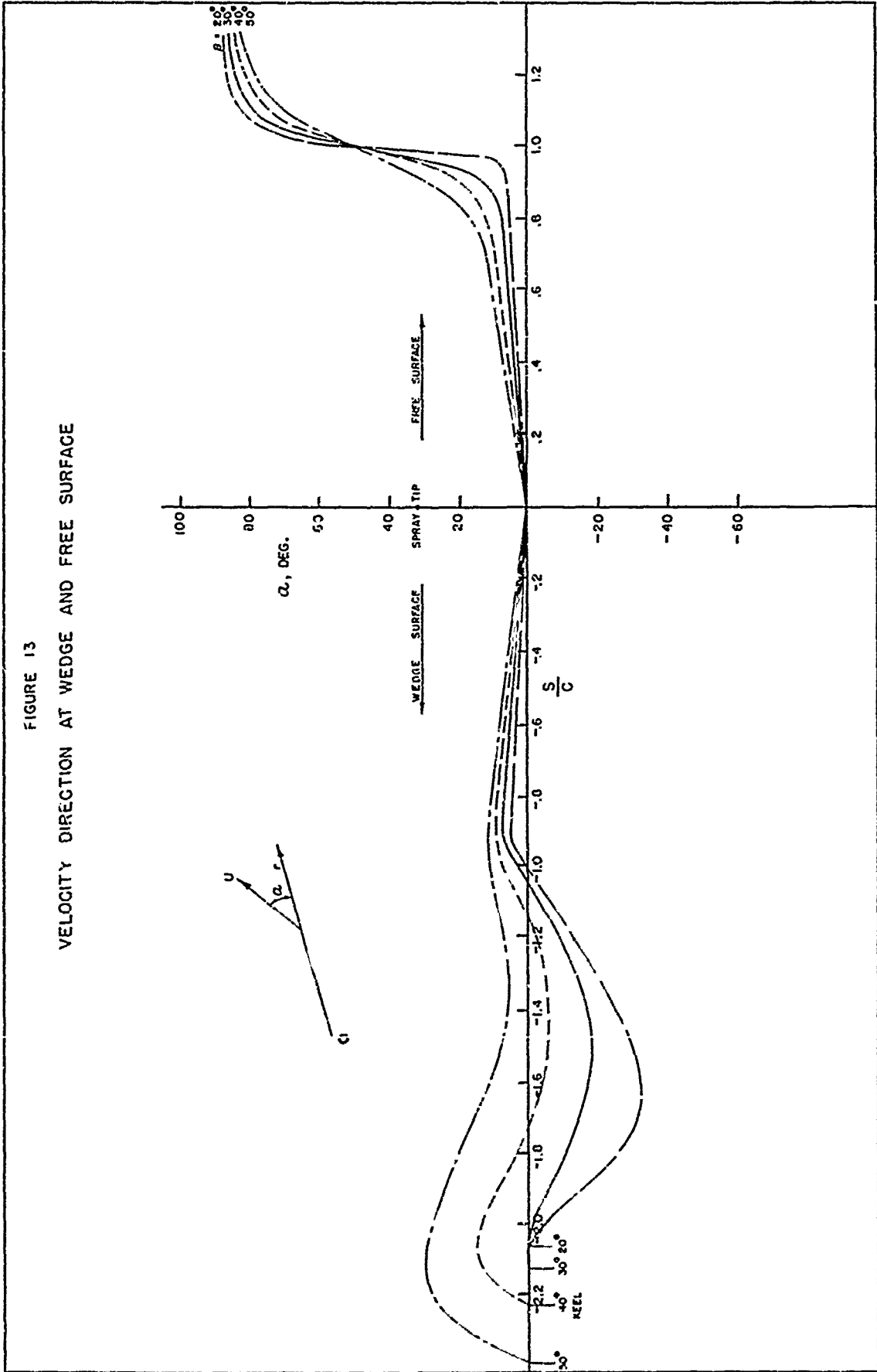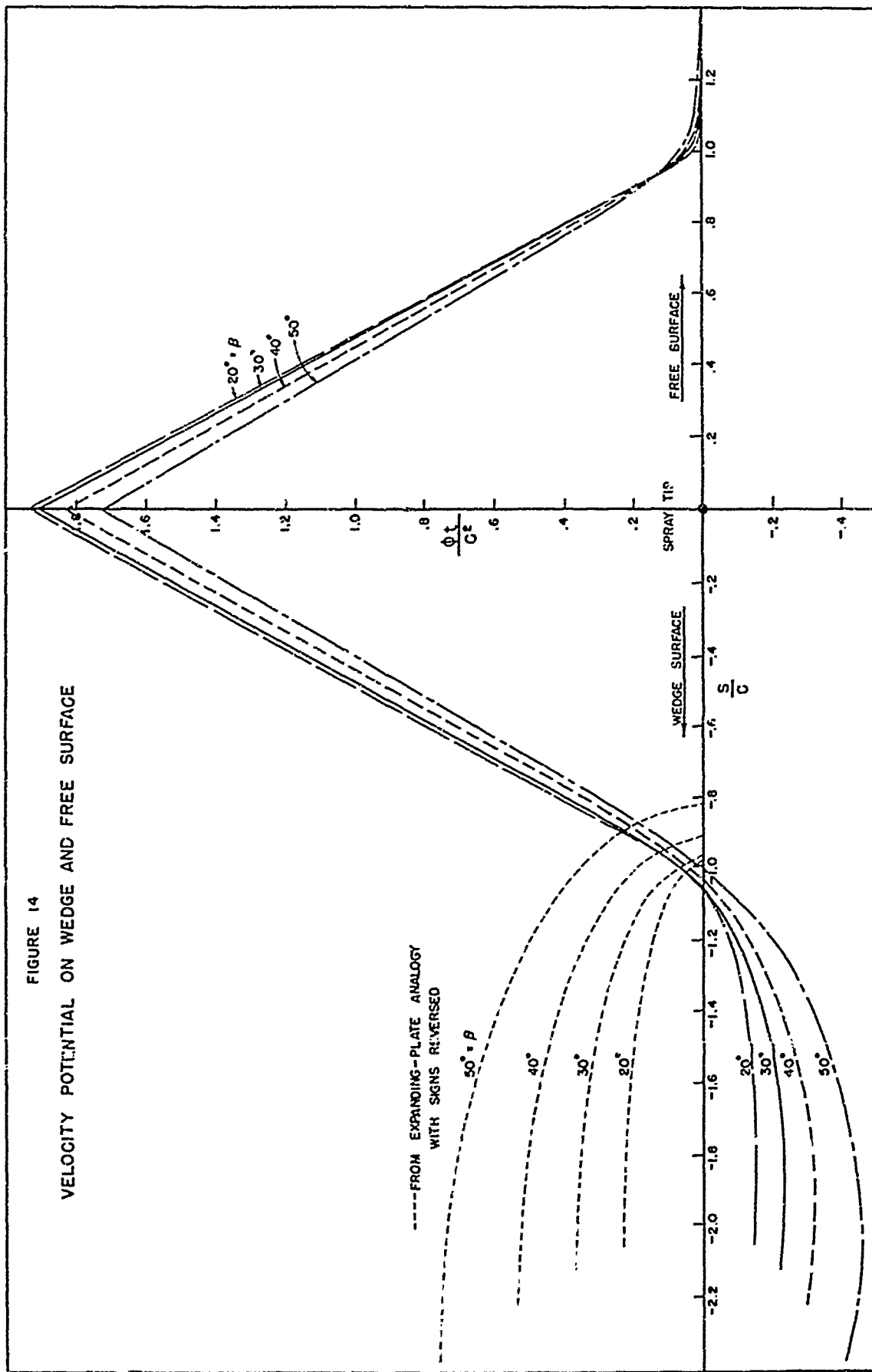
FIGURE 15

STREAM FUNCTION ALONG WEDGE AND FREE SURFACE

FIGURE 16

TANGENTIAL COMPONENT OF VELOCITY
ALONG THE WEDGE
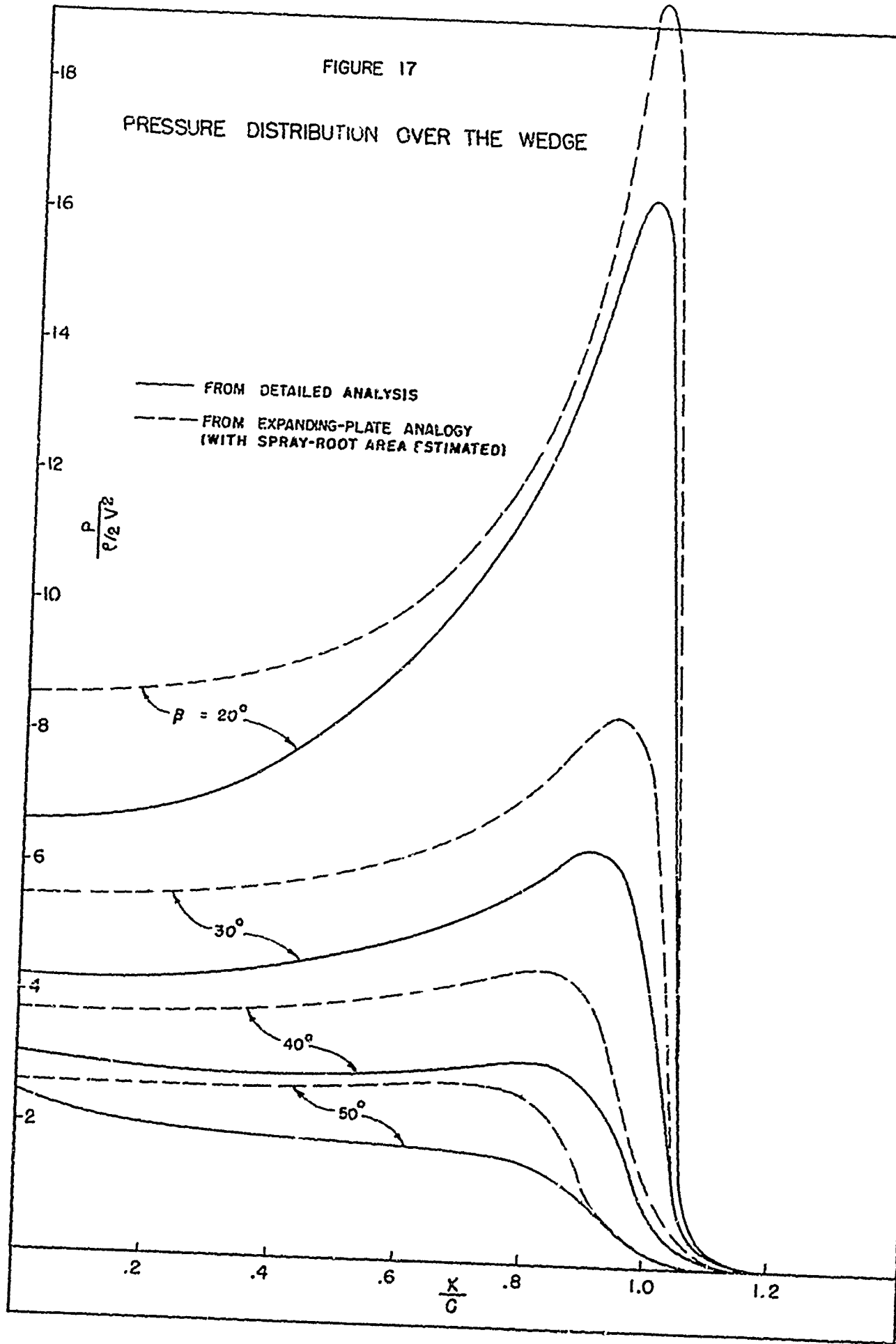
FIGURE 17

PRESSURE DISTRIBUTION OVER THE WEDGE

FIGURE 18

VARIATION OF LOAD WITH DEADRISE ANGLE
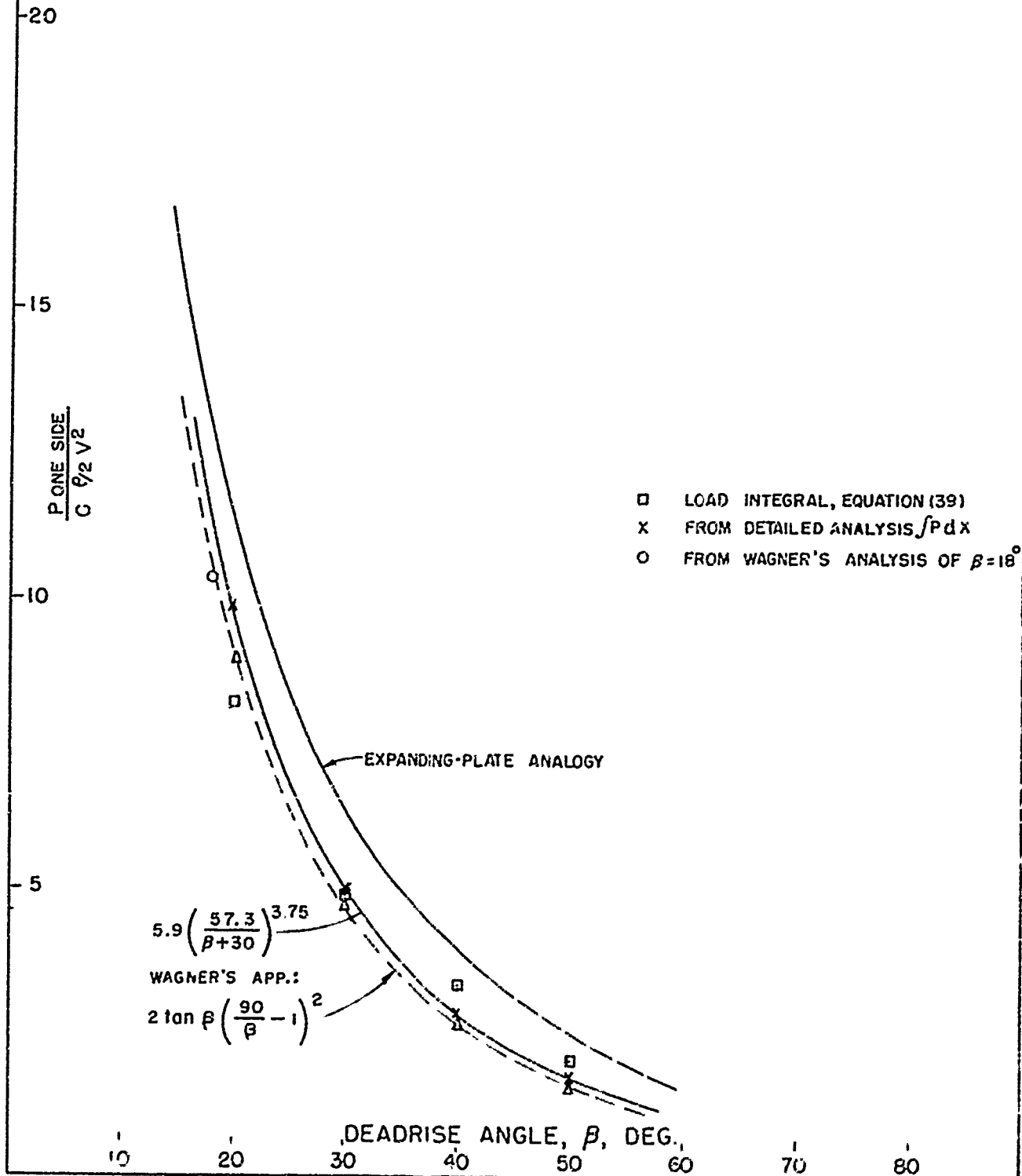FOR CONSTANT VELOCITY-WEDGE PENETRATION

FIGURE 19

PRODUCT OF POTENTIAL AND NORMAL VELOCITY
ALONG THE FREE SURFACE